Journal of Nanobiotechnology

RESEARCH

Open Access

miRNA let-7f-5p-encapsulated labial gland MSC-derived EVs ameliorate experimental Sjögren's syndrome by suppressing Th17 cells via targeting RORC/IL-17A signaling axis

Yufei Xie[1], Maosheng Chai[1], Yixiao Xing[1,2], Peiru Zhou[1*], Pan Wei[1*] and Hong Hua[1*]

Abstract

Sjögren's syndrome (SS) is an autoimmune disease primarily affecting salivary glands, with xerostomia as a distinct clinical manifestation. This disease also poses a significantly increased risk of lymphoma, severely impacting patients' quality of life. The imbalance between Th17 and Treg cells plays a critical role in SS progression, driving severe immune dysregulation, chronic inflammation, and escalating tissue dysfunction. However, current clinical treatments for SS still remain limited, and it continues to be recognized as a refractory disease. Therefore, the development of novel and effective therapeutic strategies is a pressing demand in clinical research. In recent years, extracellular vesicle (EV) therapy has emerged as a promising approach for autoimmune disease treatment, showing encouraging outcomes in modulating immune balance and alleviating symptoms. EVs carry diverse cargo, among which microRNAs (miRNAs) are highly abundant and play critical roles. These small RNAs are essential for EV-mediated functions, particularly in regulating gene expression and modulating the immune microenvironment. Our research team first isolated labial gland mesenchymal stem cells (LGMSCs) and their derived EVs (LGMSC-EVs), which offer potential therapeutic advantages in SS due to their salivary gland origin. Then we screened and identified the highly enriched miRNA let-7f-5p as a key regulator through miRNA profiling analysis. To achieve better therapeutic outcomes, we transfected exogenous miRNA let-7f-5p into LGMSC-EVs to upregulate its expression, thereby constructing let-7f-5p-encapsulated LGMSC-EVs. These modified EVs were subsequently tested in an experimental SS mouse model to evaluate their therapeutic potential. The upregulation of miRNA let-7f-5p in LGMSC-EVs significantly enhanced their therapeutic effects, resulting in clinical improvements such as increased salivary flow and reduced lymphocytic infiltration. Mechanistically, let-7f-5p-encapsulated LGMSC-EVs suppressed Th17 cells by directly targeting the 3'-untranslated region (3'UTR) of *RORC*, inhibiting the RORC/IL-17A signaling axis, and reducing IL-17A production, thereby restoring Th17/Treg balance and promoting an anti-inflammatory profile. Collectively, this let-7f-5p-encapsulated LGMSC-EV therapy offers a promising target-driven approach for the treatment of SS, achieving improved clinical outcomes and immune rebalance after modification with miRNA let-7f-5p, which presents new potential for the clinical treatment of SS.

*Correspondence:
Peiru Zhou
zhoupeiru1989@bjmu.edu.cn
Pan Wei
dent_wei@163.com
Hong Hua
honghua1968@aliyun.com
Full list of author information is available at the end of the article

Keywords Sjögren's syndrome, MicroRNA let-7f-5p, LGMSC-EVs, Th17/Treg balance, RORC/IL-17A axis

Graphical Abstract

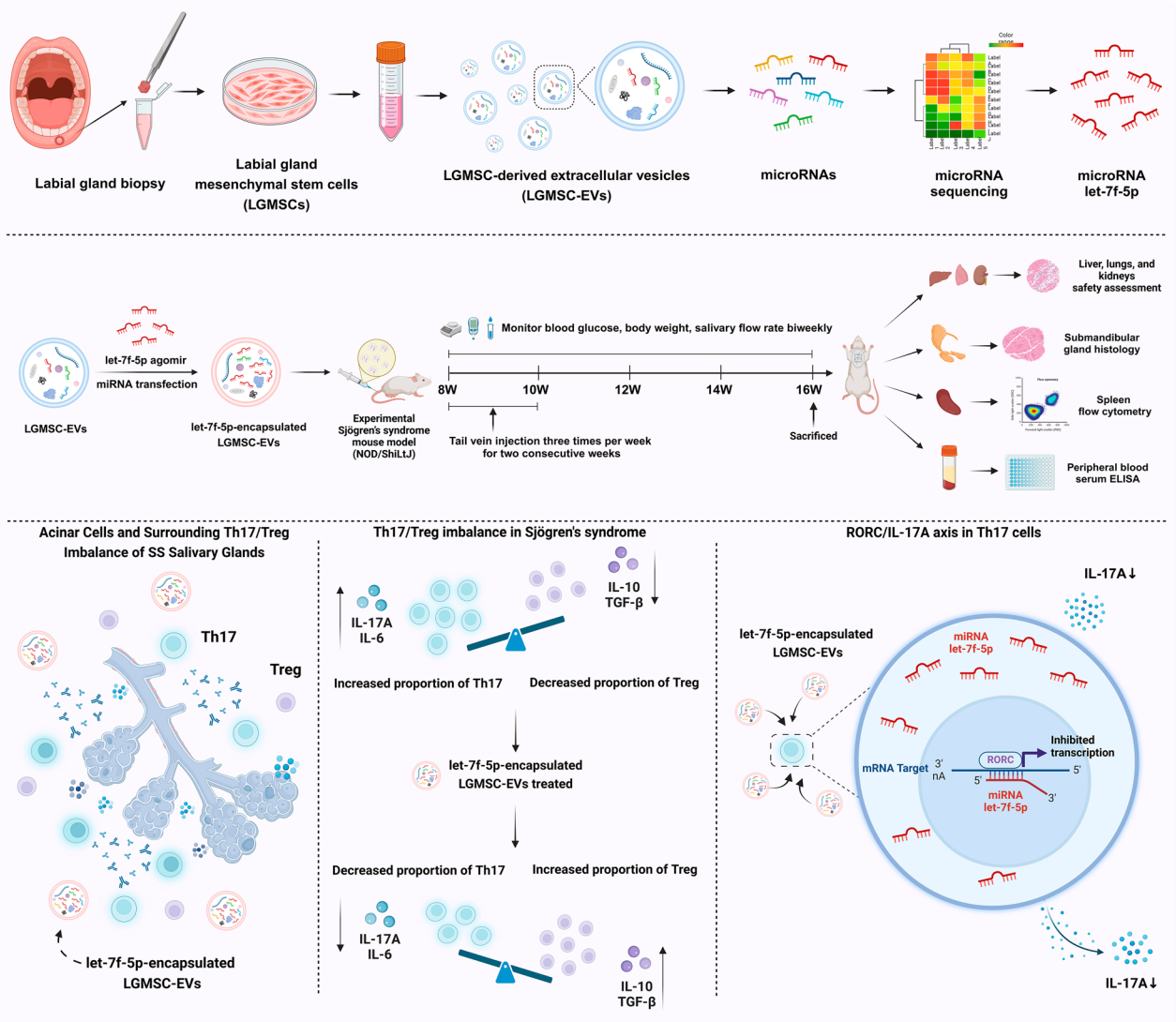

Introduction

Sjögren's syndrome (SS) is a chronic autoimmune disease characterized by progressive damage and dysfunction of the salivary gland and other exocrine glands, typically manifesting with symptoms such as xerostomia and xerophthalmia [1, 2]. Epidemiological data indicate that the prevalence of SS in China ranges from 0.3% to 0.7%, affecting an estimated 4.5 to 10 million individuals [2, 3]. SS predominantly affects women, with a male-to-female ratio of approximately 1:9 to 1:10, and the average age of onset is around 55 years [2, 4]. In addition to glandular dysfunction, SS significantly increases the risk of systemic complications, including a markedly elevated risk of lymphoma, which poses a serious threat to patient health [5–7]. Additionally, 30% to 40% of SS patients experience systemic manifestations such as synovitis, peripheral

neuropathy, and interstitial nephritis [8]. These complications severely affect patients' overall quality of life.

The pathogenesis of SS is intricate and multifactorial, with growing evidence underscoring the critical role of Th17/Treg imbalance in disease progression [9, 10]. Th17 cells, primarily known for their pro-inflammatory effects via the secretion of interleukin-17A (IL-17A), are elevated in SS patients, contributing to chronic inflammation and lymphocytic infiltration in salivary glands [11, 12]. As a key driver of dysregulated immune responses, Th17 cells play a central role in the onset and progression of SS [13]. Treg cells, which maintain immune tolerance and regulate inflammation, are often reduced or dysfunctional in SS patients, further exacerbating immune imbalance [14, 15]. This dysregulation between Th17 and Treg cells has been proved to be a key factor perpetuating the inflammatory environment and escalating salivary gland tissue damage [9, 16]. Therefore, targeting the Th17/Treg axis to modulate immune balance holds promise as a therapeutic strategy in SS management [17].

However, SS is still recognized as a refractory disease with limited treatment efficacy despite the availability of currently approved clinical therapeutic approaches [17, 18]. According to the 2020 EULAR guidelines, SS management is divided into local and systemic therapies. Local treatments primarily provide symptomatic relief, such as artificial saliva, while systemic therapies rely on immunomodulatory and immunosuppressive agents, including glucocorticoids, immunosuppressants, and biologics [19]. Although these therapies offer certain clinical benefits, long-term use often leads to significant adverse effects [20, 21]. Therefore, the development of novel and effective therapeutic strategies is a pressing demand in clinical research.

Mesenchymal stem cells (MSCs) and their extracellular vesicles (EVs) have shown considerable promise in treating autoimmune diseases due to their potent immunomodulatory abilities and regulation of the inflammatory environment [22, 23]. EVs offer distinct advantages, including reduced safety concerns, lower risk of immune rejection, easier modification for targeted delivery, and easier storage, making them particularly promising for therapeutic applications [24, 25]. Our team first isolated and characterized labial gland MSCs (LGMSCs) and their EVs (LGMSC-EVs), which offer potential therapeutic advantages in SS due to their salivary gland origin, accessibility, minimal invasiveness, and tissue specificity [26–28]. Our preliminary studies also indicate that LGMSC-EVs can effectively improve clinical symptoms in the well-established and widely used experimental SS mouse model (NOD/ShiLtJ mice), increase their salivary flow rates, reduce lymphocytic infiltration in the submandibular glands, and regulate immune responses. However, the mechanisms, particularly their role in targeting Th17 cells and restoring the Th17/Treg balance, remain to be elucidated.

EVs carry functional cargo, including proteins, RNA, and lipids, which facilitate intercellular communication, with microRNAs (miRNAs) being a particularly enriched and essential component [29]. These small RNAs are protected from degradation by plasma ribonucleases within EVs and are efficiently delivered to recipient cells. miRNAs serve as post-transcriptional regulators, binding to the 3' untranslated regions (3'UTR) of target mRNAs to modulate gene expression [30]. Through this mechanism, EV-derived miRNAs influence a wide range of cellular processes, including immune cell differentiation, cytokine production, and inflammatory signaling pathways, making them key mediators of immune regulation and modulators of the immune microenvironment [31].

In this study, we screened and identified miRNA let-7f-5p as a key regulator enriched within LGMSC-EVs that modulates the Th17/Treg balance in SS. To enhance the efficacy of LGMSC-EVs, we encapsulated exogenous miRNA let-7f-5p into LGMSC-EVs, leading to its overexpression, thereby constructing let-7f-5p-encapsulated LGMSC-EVs. These modified EVs were evaluated both in vitro and in vivo to assess their therapeutic potentials and elucidate the underlying mechanisms. In NOD/ShiLtJ mice, the administration of let-7f-5p-encapsulated LGMSC-EVs led to improved clinical outcomes, including increased salivary flow and reduced lymphocytic infiltration in submandibular glands, without inducing toxicity in major organs. Mechanistically, let-7f-5p-encapsulated LGMSC-EVs suppressed Th17 cells by directly targeting the 3'UTR of *RORC*, inhibiting the RORC/IL-17A signaling axis, and reducing IL-17A production, further contributing to the restoration of Th17/Treg balance and the reshaping of the immune microenvironment. This target-driven strategy offers a promising therapy option for SS with better clinical outcomes and immune rebalance after modifying LGMSC-EVs with miRNA let-7f-5p, presenting new potential for future clinical applications.

Materials and methods

Ethics statement

The protocol for collecting human labial gland tissues and peripheral blood was reviewed and approved by the Ethics Committee of the Peking University School and Hospital of Stomatology, Beijing, China (Approval No. PKUSSIRB-202498061). Informed consent was obtained from all participants prior to sample collection. The animal care and experimental procedures were approved by the Institutional Animal Care and Use Committee

(IACUC) of Peking University Health Science Center, Beijing, China (Approval No. DLASBD0218). All procedures were conducted in accordance with current legislative regulations and the NIH guidelines for the care and use of laboratory animals.

Subjects and samples

LGMSCs were isolated from surplus biopsy tissues of patients diagnosed with labial mucous cysts at the Department of Oral Medicine, Peking University School and Hospital of Stomatology. The use of these surplus tissues ensured that no additional harm was inflicted on the patients. All participants were in good general health, without systemic disease, and had not used immunomodulatory drugs in the past year. SS patients were selected according to the 2002 American-European Consensus Group (AECG) diagnostic criteria for Sjögren's syndrome and had not received prior systemic treatment or medications that could influence immune function. Exclusion criteria included the presence of other systemic diseases, active infections, or surgical contraindications to ensure consistency and reliability of the results. Only patients who provided informed consent were included in the study.

Isolation and culture of LGMSCs

Labial gland tissues located adjacent to mucoceles were obtained during surgical excision procedures. These tissues were promptly rinsed with phosphate-buffered saline (PBS) to remove residual blood and connective tissues. The cleaned tissue samples were then cut into small fragments using sterile surgical scissors and transferred to culture flasks containing alpha-Minimum Essential Medium (α-MEM) (Gibco, USA), supplemented with 15% fetal bovine serum (FBS) (Gibco, USA) and 1% penicillin–streptomycin (Beyotime, China). Cultures were maintained at 37 °C in a humidified 5% CO_2 incubator, and the medium was refreshed every 3 days to optimize cell growth. Once the cultures reached 80–90% confluence, adherent cells were detached using 0.25% trypsin–EDTA (Gibco, USA) and subcultured. Cells between passages 3 and 5 were used for all downstream experiments to ensure reproducibility and maintain cellular characteristics.

Characterization of LGMSCs

Surface marker analysis via flow cytometry

The surface markers of third-passage LGMSCs were assessed by flow cytometry. Cells were digested, centrifuged, and resuspended in PBS at a concentration of 1×10^7 cells/mL. A 100 µL cell suspension was incubated with antibodies specific to CD29, CD73, CD90, CD105, CD31, CD45, CD80, CD86, and HLA-DR (BD Biosciences, USA) or corresponding isotype controls for 30 min at 4 °C in the dark. Following incubation, cells were washed twice with PBS and resuspended in 200 µL of flow cytometry staining buffer for analysis. Data were acquired using a FACSCalibur flow cytometer (BD Pharmingen, USA), and processed with FlowJo software (Tree Star, USA).

Osteogenic differentiation

To induce osteogenic differentiation, LGMSCs were cultured in osteogenic induction medium (iCell, China) according to the manufacturer's instructions. Cells were seeded at a density of 10,000 cells/cm [2] in 6-well culture plates and maintained with medium changes every 2 days. After 21 days, the induction was terminated, and the cells were fixed with 4% formaldehyde in PBS for 30 min at room temperature. Calcium deposits, indicating successful osteogenesis, were visualized by staining with Alizarin Red solution for 10 min, followed by extensive washing with PBS to remove excess stain. The stained cells were analyzed and imaged using a light microscope (Leica DMIRB, Germany).

Adipogenic differentiation

Adipogenic differentiation of third-passage LGMSCs was induced using adipogenic induction medium (Pricella, China) for 14 days, with medium changes every 2 to 3 days. Following the induction period, cells were fixed in 4% formaldehyde for 30 min at room temperature. To assess lipid accumulation, cells were stained with Oil Red O solution for 30 min according to the manufacturer's instructions. Stained cells were observed under a light microscope to confirm intracellular lipid droplet formation, indicating successful adipogenic differentiation.

Chondrogenic differentiation

Third-passage LGMSCs were cultured in chondrogenic induction medium (Pricella, China) for 21 days to evaluate chondrogenic differentiation. The 100 mL medium supplemented with 100 µL sodium pyruvate, 100 µL proline, 10 µL dexamethasone, 300 µL ascorbic acid, 100 µL ITS supplement, and 1 mL TGF-β3. The medium was refreshed every 3 days to maintain optimal conditions. After the induction period, cell aggregates were fixed in formalin for 20 min at room temperature. Chondrogenic differentiation was confirmed by staining the aggregates with Alcian Blue and Safranin O for 30 min to visualize the cartilaginous matrix. Stained samples were examined

under a light microscope to assess the formation of cartilaginous extracellular matrix.

Isolation of LGMSC-EVs

LGMSCs were cultured in α-MEM supplemented with 10% exosome-depleted FBS for 72 h. After the culture period, the conditioned medium was collected and sequentially centrifuged at 300×*g* for 10 min, 2000×*g* for 10 min, and 10,000×*g* for 30 min to remove cells, large vesicles, and debris. The supernatants were then concentrated using Amicon Ultra-15 centrifugal filters (Millipore, USA) at 5000×*g* for 30 min. The concentrated samples were layered onto a 30% sucrose/deuterium oxide (D_2O) cushion (Macklin, China) and ultracentrifuged at 100,000×*g* for 70 min at 4 °C using an SW32Ti rotor in an Optima L-100XP ultracentrifuge (Beckman Coulter, USA). The exosome-enriched sucrose/D_2O cushion was collected, resuspended in PBS, and centrifuged at 5,000×*g* for 30 min 3 times to remove residual sucrose. The purified LGMSC-EVs were resuspended in PBS and stored at − 80 °C. Protein concentration was measured using a BCA protein assay kit (Solarbio, China).

Characterization of LGMSC-EVs

Transmission electron microscopy (TEM)

To assess the morphology of LGMSC-EVs, TEM was performed. Purified exosome samples were diluted to a concentration of approximately 1×10^{11} vesicles/mL in PBS. A 10 μL aliquot of the diluted sample was placed onto a 200-mesh formvar carbon-coated copper grid and allowed to settle for 5 min at room temperature. Excess liquid was carefully removed with filter paper, and the grid was stained with 1% phosphotungstic acid for 2 min. After blotting away the excess stain and air-drying at room temperature, the grid was examined using a JEM-1400 transmission electron microscope (JOEL, Japan) to capture the EV images.

Nanoparticle tracking analysis (NTA)

The particle size distribution and concentration of LGMSC-EVs were evaluated using NTA on a ZetaView PMX 110 instrument (Particle Metrix, Germany) equipped with a 405 nm laser. Exosome samples were diluted in PBS to an optimal concentration range of 1×10^7 to 1×10^9 vesicles/mL to ensure accurate measurement. Each sample was recorded as a 60-s video at a frame rate of 30 frames per second. The ZetaView software (version 8.02.28) was used to analyze particle movement, providing data on mean, mode, median particle size, and concentration, ensuring reliable quantification and quality assessment of LGMSC-EVs.

Capillary western blotting

Characterization of LGMSC-EVs was performed using an automated capillary electrophoresis western blotting system (WES™, ProteinSimple, USA) [32, 33]. Protein lysates (1 mg/mL) were prepared by mixing 5.6 μL of the sample with 1.4 μL of fluorescent master mix and denatured at 95 °C for 5 min. The lysates, along with blocking reagent, primary antibodies (1:1000 dilution of anti-CD63, anti-CD81, anti-TSG101, and anti-Calnexin; Abcam, UK), secondary HRP-conjugated antibodies, and chemiluminescent substrate, were loaded into the manufacturer's microplate. The WES system automatically conducted electrophoretic separation and immunodetection using a 12–230 kDa separation module under default settings. Chemiluminescence was detected through an exposure series for optimal signal capture. Data analysis was conducted with Compass software (ProteinSimple, USA), producing electropherograms and virtual blot images to quantify the chemiluminescence signal for comparative purposes.

Mice and treatment protocol

Six-week-old female NOD/ShiLtJ mice were obtained from GemPharmatech (Nanjing, China), and six-week-old female BALB/c mice were supplied by the Peking University Laboratory Animal Center (Beijing, China). All mice were maintained in a specific pathogen-free (SPF) environment under controlled temperature and humidity, with unrestricted access to standard rodent chow and water. All animal care and experimental procedures were conducted in accordance with institutional ethical guidelines to ensure the welfare and humane treatment of the animals.

The dosage and frequency of LGMSC-EV and let-7f-5p-encapsulated LGMSC-EV administration were based on established protocols from previous studies [27, 28]. Eight-week-old female NOD/ShiLtJ mice received intravenous tail vein injections of LGMSC-EVs at a dose of 100 μg/mouse, diluted in 200 μL of PBS, administered 3 times per week for 2 consecutive weeks. The positive control group received hydroxychloroquine (HCQ) via oral gavage, while the negative control group received equivalent volumes of PBS via tail vein injection. Body weight, serum glucose levels, and salivary flow rates were monitored biweekly throughout the treatment period. At 16 weeks of age, the mice were euthanized, and submandibular glands, spleens, and peripheral blood serum were collected for further analysis. All procedures adhered to institutional ethical guidelines for animal care and experimentation.

Salivary flow rate measurement

The method for measuring salivary flow rate was adapted from established protocols used in our previous experiments and relevant literature [27, 28, 34, 35]. The salivary flow rate was assessed biweekly throughout the study. Mice were anesthetized with 1.25% tribromoethanol at a dose of 0.175 mL/10 g body weight (Aibei Biotechnology, China) to ensure minimal discomfort. Following anesthesia, pilocarpine (5 mg/kg body weight; MCE, USA) was administered intraperitoneally to stimulate salivation. 5 min post-administration, stimulated saliva was collected from the oral cavity over a 15 min period. The collected saliva was weighed using a precision balance (Mettler Toledo, Switzerland). The salivary flow rate was calculated as follows: salivary flow rate (mg/min/g) = saliva mass (mg)/[collection time (min) × body weight (g)].

Histopathological analysis of salivary glands

Following euthanasia, submandibular salivary glands were carefully dissected and immediately fixed in 10% neutral buffered formalin for 24 h at room temperature. The fixed tissues were subsequently dehydrated, embedded in paraffin, and sectioned at a thickness of 4 μm. Sections were stained with hematoxylin and eosin (H&E) following standard histopathological procedures to evaluate inflammation and lymphocytic infiltration within the glandular structures. Histological evaluation was conducted using a light microscope, with multiple randomly selected fields examined to comprehensively assess the distribution and extent of inflammatory cell infiltration. According to the H&E staining results, a commonly used scoring system based on the density and number of infiltrated lymphocytic foci was employed to assess the severity of tissue damage [36]. A lymphocytic focus was defined as a group of ≥ 50 lymphocytes per 4 mm^2 of gland tissue.

Safety evaluation of LGMSC-EVs and let-7f-5p-encapsulated LGMSC-EVs

To evaluate the safety profile of LGMSC-EVs and let-7f-5p-encapsulated LGMSC-EVs in vivo, the liver, lung, and kidney tissues were collected for histopathological examination. The experiment was carried out according to the protocol described in previous studies. At 16 weeks, the mice were euthanized, and the collected organs were fixed in 4% paraformaldehyde, paraffin-embedded, sectioned at 4 μm, and stained with H&E. Histopathological analysis was conducted under a light microscope to identify potential toxicity or structural changes, providing a comprehensive safety assessment.

Flow cytometry

The proportions of Th17 and Treg cells were evaluated using flow cytometry. For spleen analysis, the spleens from mice were excised and processed to isolate lymphocytes. The tissue was finely minced, and approximately 2 mL of erythrocyte lysis buffer (BioLegend, USA) was added to the cell suspension for 2 min to remove red blood cells. The cells were then washed and resuspended in RPMI 1640 medium at a final concentration of 2×10^6 cells/mL. For PBMC analysis from SS patients, cells were collected following 72 h of co-culture with LGMSC-EVs and adjusted to a concentration of 2×10^6 cells/mL before staining. Th17 cells were defined as $CD4^+IL\text{-}17A^+$, while Treg cells were characterized as $CD4^+CD25^+Foxp3^+$. To detect Th17 cells, cells were stimulated for 5 h at 37 °C in a 5% CO_2 environment using Leukocyte Activation Cocktail (BD Pharmingen, USA) prior to intracellular staining. After stimulation, cells were fixed and permeabilized using the Intracellular Fixation and Permeabilization Buffer Set (eBioscience, USA), followed by staining with anti-CD4-FITC and anti-IL-17A-APC antibodies (Biolegend, USA) for 1 h at room temperature. For Treg cell analysis, cells were stained with anti-CD4-FITC, anti-CD25-APC, and anti-Foxp3-PE antibodies (BD Pharmingen, USA) at room temperature for 1 h. The samples were analyzed using a FACSCalibur flow cytometer, and data were processed with FlowJo software.

Enzyme-linked immunosorbent assay (ELISA)

The concentrations of IL-6, IL-17A, IL-10, and TGF-β were measured in mouse serum and human PBMC culture supernatants using ELISA kits (MEIMIAN, China) according to the manufacturer's protocols. Peripheral blood was collected from mice, and serum was separated by centrifugation. Supernatants from PBMC co-cultures were collected after 72 h of incubation. All samples were stored at − 80 °C until analysis. Cytokine levels were quantified based on the respective standard curves generated in each assay, with absorbance readings obtained via a microplate reader.

miRNA sequencing and analysis

The high-throughput sequencing and analysis of miRNAs in LGMSC-EVs were conducted as previously described [28]. Differentially expressed miRNAs were screened by Shanghai Biotechnology Corporation (Shanghai, China). Total RNA extraction, library construction, and sequencing on the Illumina HiSeq platform were performed according to the manufacturer's instructions. Clean reads were generated after filtering raw sequencing data and aligned to the human reference genome. Differential expression analysis was conducted using

DESeq2, with a significance threshold set at fold change ≥ 1.5 and p-value < 0.05. Gene Ontology (GO) and Kyoto Encyclopedia of Genes and Genomes (KEGG) enrichment analyses were performed to explore the biological functions and pathways associated with differentially expressed miRNAs. Data visualization was conducted using an online bioinformatics platform (https://www.omicsmart.com/#/). Target gene prediction was carried out with online tools, including TargetScan (https://www.targetscan.org/vert_80/) and miRDB (https://mirdb.org/). Only target genes identified by both of the prediction programs were accepted.

miRNA Transfection and evaluation of transfection efficacy

miRNA let-7f-5p mimic, let-7f-5p inhibitor, NC mimic for in vitro studies, as well as miRNA let-7f-5p agomir, let-7f-5p antagomir, and NC agomir for in vivo studies, were synthesized by RiboBio (Guangzhou, China). miRNA Transfection was performed using the Exo-Fect™ Exosome Transfection Kit (System Biosciences, USA) according to the manufacturer's protocol. Briefly, 50–300 μg of exosome protein (about 1×10^6) suspended in 50 μL of PBS were mixed with Exo-Fect solution and the corresponding miRNA mimic or inhibitor. The reaction mixture was incubated at 37 °C for 10 min with gentle inversion and then immediately placed on ice. ExoQuick-TC reagent was added to stop the reaction, followed by incubation at 4 °C for 30 min. The transfected exosomes were pelleted by centrifugation at 13,000 × g for 3 min, the supernatant was removed, and the exosome pellets were resuspended in 300 μL of PBS for storage at − 80 ℃ until use.

To assess the miRNA transfection efficacy, total miRNA was extracted from transfected LGMSC-EVs using the miRcute Serum/Plasma miRNA Isolation Kit (TIANGEN, China). The isolated miRNA was reverse transcribed into cDNA using the miRcute Plus miRNA First-Strand cDNA Kit (TIANGEN, China) according to the manufacturer's instructions. Quantitative real-time PCR (qRT-PCR) was conducted using the miRcute Plus miRNA Qpcr SYBR Green Kit (TIANGEN, China) with specific primers for the target miRNA. U6 small nuclear RNA was used as an internal control. Relative miRNA expression levels were quantified using the $2^{-\Delta\Delta Ct}$ method to confirm successful transfection compared to non-transfected controls. Primer sequences for mir-let-7f-5p probe and U6 were listed in Supplementary Material 1.

Isolation of human PBMCs from SS patients and their co-culture with LGMSC-EVs

PBMCs were isolated from peripheral blood samples of SS patients using Ficoll density-gradient centrifugation (Solarbio, China). Peripheral blood was layered over Ficoll-Paque and centrifuged for 20 min in a swing-out rotor without applying a brake. The mononuclear cell layer at the plasma-Ficoll interface was collected, transferred to a new tube, washed with PBS, and centrifuged again for 10 min. The resulting pellet was resuspended in complete RPMI 1640 medium (Gibco, USA). For co-culture experiments, PBMCs were activated with anti-CD3 antibody and anti-CD28 antibody (BioLegend, USA) to induce T cell activation. Following activation, PBMCs were plated at an appropriate density and treated with LGMSC-EVs at a final concentration of 100 μg/mL, according to prior protocols. Co-cultures were maintained in complete RPMI 1640 medium for 72 h. Post-incubation, cells were collected for flow cytometry analysis, and supernatants were harvested for ELISA assays.

Th17 cell enrichment via magnetic bead sorting

Th17 cell isolation was performed using the Human IL-17 Secretion Assay—Cell Enrichment and Detection Kit (Miltenyi Biotec, Germany) according to the manufacturer's instructions. Human PBMCs were initially stimulated with Leukocyte Activation Cocktail (BD Pharmingen, USA) at 37 °C for 4 h to induce IL-17 secretion. After stimulation, cells were washed and incubated with an IL-17-specific catch reagent at 37 °C for 45 min to bind secreted IL-17 to the cell surface. Subsequently, the cells were labeled with IL-17 detection antibody (PE) and incubated with anti-PE microbeads ultrapure for magnetic labeling. The cell suspension was passed through a MACS column within a magnetic field generated by a MACS separator (Miltenyi Biotec, Germany), allowing IL-17-positive Th17 cells to be retained. Non-labeled cells were washed out, and IL-17-secreting Th17 cells remained bound to the column. Finally, the column was removed from the magnetic field, and Th17 cells were eluted using autoMACS Rinsing Solution (Miltenyi Biotec, Germany). This method provided high specificity and efficiency for isolating IL-17-secreting Th17 cells for further analysis.

Dual-luciferase reporter assay

To evaluate the regulatory effect of miRNA let-7f-5p on the *RORC* 3'UTR, a dual-luciferase reporter assay was performed using the pmirGLO Dual-Luciferase miRNA Target Expression Vector (Promega, USA). Wild-type (WT) and mutant (MUT) 3'UTR sequences of *RORC* were synthesized (RiboBio, China) and inserted downstream of the firefly luciferase gene in the pmirGLO vector. HEK293T cells were seeded in 96-well plates and incubated overnight. Co-transfection of the luciferase reporter constructs with either let-7f-5p mimic or

NC mimic was conducted using Lipofectamine 2000 (Invitrogen, China). 48 h after transfection, luciferase activity was measured using the Dual-Glo Luciferase Assay System (Promega, USA). Firefly luciferase (fLuc) activity was normalized to Renilla luciferase (rLuc) activity to control for transfection efficiency. The ratio of fLuc to rLuc was calculated to quantify relative dual-luciferase activity. Each experiment was performed in triplicate to ensure statistical reliability.

qRT-PCR analysis of *RORC* and *IL-17A* mRNA expression in Th17 Cells

Total RNA was isolated from Th17 cells using TRIzol reagent (Invitrogen, USA) in accordance with the manufacturer's protocol. RNA concentration and purity were assessed by measuring the OD260/OD280 ratio with a NanoDrop 2000 spectrophotometer (Thermo Fisher Scientific, USA). One microgram of total RNA was reverse-transcribed into cDNA using the ABScript III RT Master Mix (ABclonal, China), following the supplier's guidelines, and stored at − 20 °C until further analysis. qRT-PCR was conducted using 2X Universal SYBR Green Fast qPCR Mix (ABclonal, China) in a 20 μL reaction volume. The amplification protocol included an initial denaturation at 95 °C for 3 min, followed by 40 cycles of 95 °C for 5 s and 60 °C for 30 s. The housekeeping gene β-actin served as an internal control to normalize mRNA expression levels. Relative expression levels of *RORC* and *IL-17A* mRNA were quantified using the $2^{-\Delta\Delta Ct}$ method. Primer sequences for *RORC*, *IL-17A*, and β-actin were listed in Supplementary Material 2.

Capillary western blot analysis of RORγT and IL-17A in Th17 cells

Capillary western blotting was performed to assess the protein expression levels of RORγT and IL-17A in Th17 cells. Protein lysates were extracted from the cells, and their concentration was quantified using a BCA protein assay kit (NCM Biotech, China). The samples were diluted to the required concentration, combined with a fluorescent master mix, and denatured at 95 °C for 5 min. Prepared lysates were loaded into the capillary electrophoresis system (WES™, ProteinSimple, USA), along with blocking reagents, primary antibodies targeting RORC (1:500, Bioss, China), IL-17A (1:500, Bioss, China), HRP-conjugated secondary antibodies, and a chemiluminescent substrate. The assay was conducted following the system's standard protocol. Protein bands were visualized, and their expression was quantitatively analyzed using Compass software (ProteinSimple, USA). β-actin (1:4000, Proteintech, China) was used as the internal control for normalizing protein expression levels.

Immunohistochemistry and immunofluorescence analysis

IHC and IF staining were performed to evaluate the expression of RORγT and IL-17A in submandibular gland tissues of NOD/ShiLtJ mice. For IHC, paraffin-embedded sections were deparaffinized, rehydrated, and treated with 3% hydrogen peroxide for endogenous peroxidase blockade. Antigen retrieval was conducted using citrate buffer under high temperatures. Sections were then blocked with 5% BSA and incubated overnight at 4 °C with primary antibodies against RORγT (1:100, Bioss, China) and IL-17A (1:100, Bioss, China). The next day, HRP-conjugated secondary antibodies were applied, and staining was visualized using DAB solution (ZSGB-BIO, China), followed by hematoxylin counterstaining. Images were captured using a light microscope (Nikon, Japan). Immunohistochemical scores (histoscores) were calculated by combining 2 parameters: staining intensity and the percentage of positive cells. Staining intensity was graded on a 4-point scale: 0 for no staining (negative), 1 for light yellow (weak positive), 2 for brown yellow (positive), and 3 for dark brown (strong positive). The percentage of positive cells was also graded on a 4-point scale: 1 for ≤ 25%, 2 for 26–50%, 3 for 51–75%, and 4 for > 75%. The final histoscore was obtained by multiplying these two scores.

For IF staining, sections were similarly blocked and incubated with primary antibodies overnight at 4 °C, followed by incubation with fluorophore-conjugated secondary antibodies (MXB, China) for 1 h at room temperature. Nuclei were counterstained with DAPI. Fluorescent images were acquired using a fluorescence microscope and scanned with a Panoramic Digital Slide Scanner (3DHISTECH, Hungary).

Statistical analysis

All experimental data are expressed as the mean ± standard error of the mean (SEM) based on at least 3 independent experiments. Statistical analyses were performed using IBM SPSS Statistics for Windows, version 26.0 (IBM Corp., USA). The normality of data distribution was evaluated with the Kolmogorov–Smirnov test. For comparisons between 2 groups, an independent, unpaired two-tailed Student's *t*-test was applied. For multiple group comparisons, one-way analysis of variance (ANOVA) followed by the Tukey test was used when data showed normal distribution and homogeneity of variances. For data that did not meet these criteria, the Dunnett T3 test was conducted. Statistical significance was defined as a *p*-value of less than 0.05, with significance levels indicated as $^{*}p < 0.05$, $^{**}p < 0.01$, $^{***}p < 0.001$, and ns means no significance.

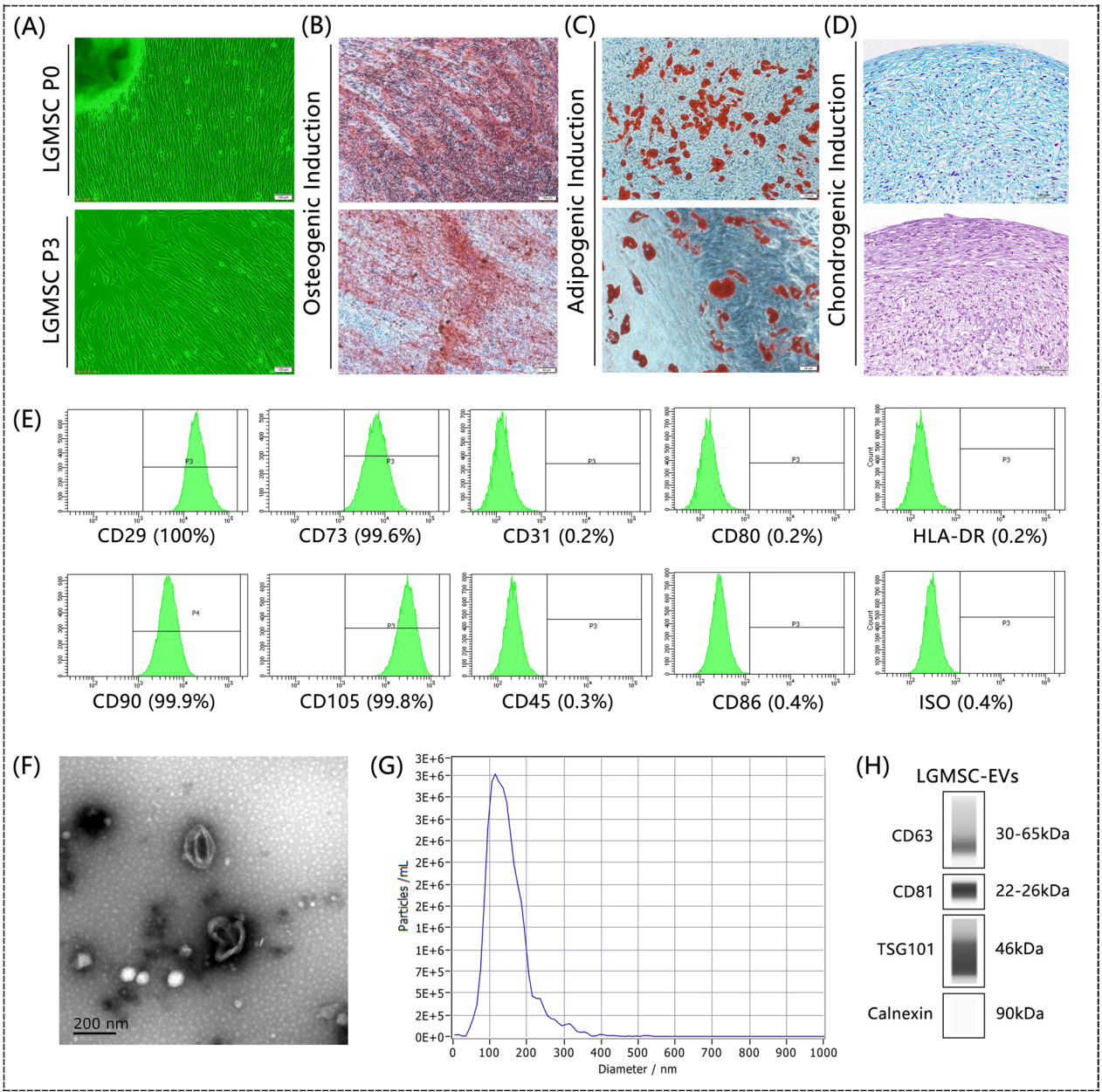

Fig. 1 Isolation and Characterization of LGMSCs and LGMSC-EVs. **A** LGMSCs isolated from human labial gland tissues show the characteristic spindle-shaped morphology typical of MSCs. **B**–**D** The multipotent capacity of LGMSCs is confirmed by successful differentiation into osteogenic (**B**, Alizarin Red staining), adipogenic (**C**, Oil Red O staining), and chondrogenic lineages (**D**, Alcian Blue/Safranin O staining). **E** Flow cytometry analysis shows high expression of MSC markers (CD29, CD90, CD73, CD105), with minimal expression of costimulatory molecules (CD80, CD86) and hematopoietic/endothelial markers (CD31, CD45, HLA-DR). **F** TEM image of LGMSC-EVs, demonstrating their typical cup-shaped morphology and diameter. **G** NTA of LGMSC-EVs, indicating an average particle size of 146.9 nm with a dominant peak at 124.5 nm and a concentration of 3.30×10^9 particles/mL. **H** Western blotting analysis confirmed the presence of exosome markers CD63, CD81, and TSG101, with the absence of calnexin confirming EV purity

Result

Isolation and characterization of LGMSCs and LGMSC-EVs

LGMSCs were successfully isolated from human labial gland tissues, displaying the characteristic spindle-shaped morphology typical of MSCs (Fig. 1A). The multipotent capacity of LGMSCs was confirmed by their differentiation into osteogenic, adipogenic, and chondrogenic lineages, verified through Alizarin Red, Oil Red O, and Alcian Blue/Safranin O staining, respectively (Fig. 1B–D). Flow cytometry analysis showed high

expression of key MSC markers, including CD29 (100%), CD90 (99.9%), CD73 (99.6%), and CD105 (99.8%), while the expression of costimulatory molecules (CD80: 0.2%, CD86: 0.4%) and hematopoietic/endothelial markers (CD31: 0.2%, CD45: 0.3%, HLA-DR: 0.2%) remained minimal (Fig. 1E).

LGMSC-EVs were isolated from the conditioned medium using differential ultracentrifugation and were characterized by TEM, which revealed their typical cup-shaped morphology (Fig. 1F). NTA showed an average particle size of 146.9 nm, with a dominant peak at 124.5 nm, accounting for 98.4% of the particles, and a concentration of 3.30×10^{9} particles/mL (Fig. 1G). Western blotting confirmed the presence of classical exosome markers CD63, CD81, and TSG101, while the absence of calnexin indicated the purity of the isolated vesicles (Fig. 1H).

LGMSC-EVs ameliorate experimental SS symptoms by modulating Th17/Treg balance

The typical clinical manifestations of SS include reduced salivary flow rates and lymphocytic infiltration in salivary glands. These changes are closely linked to immune dysregulation, particularly an increased Th17/Treg ratio, which is associated with the onset and progression of the disease [37]. To model these pathological and immunological features, the NOD/ShiLtJ mouse is widely used, as it exhibits progressive saliva secretion decline, lymphocytic infiltration, and an imbalance in Th17 and Treg cells [38–40]. These features make it a suitable and well-established model for studying potential therapeutic strategies for SS. Therefore, in this study, we utilized NOD/ShiLtJ mice to assess the therapeutic effects of LGMSC-EVs on SS.

Eight-week-old female NOD/ShiLtJ mice were treated with LGMSC-EVs via intravenous tail vein injections (3 times per week for 2 weeks, following the dosing regimen established in our previous studies). The positive control group received HCQ by oral gavage, while the negative control group received PBS injections. Body weight, serum glucose levels, and salivary flow rates were monitored biweekly (Fig. 2A). Intravenous administration of LGMSC-EVs significantly ameliorated experimental SS symptoms in NOD/ShiLtJ mice. During the treatment period, the body weight of the mice steadily increased with age, and blood glucose levels remained stable (Fig. 2B–C). Mice treated with LGMSC-EVs exhibited a significant increase in salivary flow rates compared to the PBS control group, with effects that began to surpass those of HCQ, a widely used clinical treatment for SS, after 12 weeks of age (Fig. 2D). Histopathological analysis of the submandibular glands revealed a significant reduction in both the number and size of lymphocytic infiltration foci ($p<0.001$), with effects comparable to HCQ treatment (Fig. 2E–F).

To investigate the immune modulation effects of LGMSC-EVs, flow cytometry was performed to quantify the proportions of Th17 and Treg cells in the spleens of treated mice (Fig. 3A–C). LGMSC-EV treatment significantly reduced the proportion of Th17 ($CD4^{+}IL\text{-}17A^{+}$) cells compared to the PBS control group, decreasing the mean Th17 percentage from 1.06% to 0.47%, representing a 56% reduction ($p=0.004$). Meanwhile, the proportion of Treg ($CD4^{+}Foxp3^{+}$) cells showed a modest increase, with the mean percentage rising from 11.50% to 12.76% ($p=0.421$). Additionally, the Th17/Treg ratio was also markedly decreased, with the mean ratio dropping from 0.092 to 0.037, a reduction of 60% compared to the control group ($p=0.012$, Fig. 3D). Hence, the shift in Th17/Treg balance can be primarily attributed to the suppression of Th17 cells by LGMSC-EVs.

Following this, we performed ELISA to measure cytokine levels in the peripheral blood serum of treated mice. The analysis demonstrated a significant reduction in the levels of IL-6 and IL-17A, accompanied by an increase in the levels of IL-10 and TGF-β (Fig. 3E–H). These findings further corroborate the immunomodulatory effects of LGMSC-EVs, highlighting their potential to restore immune balance by suppressing inflammatory responses. Moreover, assessments of the liver, kidney, and lung tissues in treated mice revealed that LGMSC-EVs showed a favorable safety profile, showing no signs of significant systemic toxicity (Fig. 3I).

miRNA let-7f-5p in LGMSC-EVs plays a key role in suppressing Th17 cells, modulating the Th17/Treg balance

Considering that LGMSC-EVs are enriched with a variety of miRNAs, and their immunoregulatory effects are largely mediated by these miRNAs, we set up to identify the key miRNA responsible for regulating the Th17/Treg balance, particularly by suppressing Th17 cells. Therefore, we performed miRNA sequencing on LGMSC-EVs. LGMSC-EVs are composed of approximately 462 miRNAs, among which 65 are identified as novel RNAs (Supplementary Material 3). The top 10 significantly upregulated miRNAs in LGMSC-EVs from healthy controls (HC) and SS patients are shown in Fig. 4A, with the top five being hsa-let-7b-5p, hsa-let-7a-5p, hsa-let-7i-5p, hsa-miR-125b-5p, and hsa-let-7f-5p. Target prediction was performed using databases such as TargetScan and miRDB. The KEGG pathway classification of the predicted gene targets for the upregulated miRNAs from LGMSC-EVs is presented in Fig. 4B, revealing that the targets are predominantly enriched in immune system-related pathways, ranking the second. Through flow

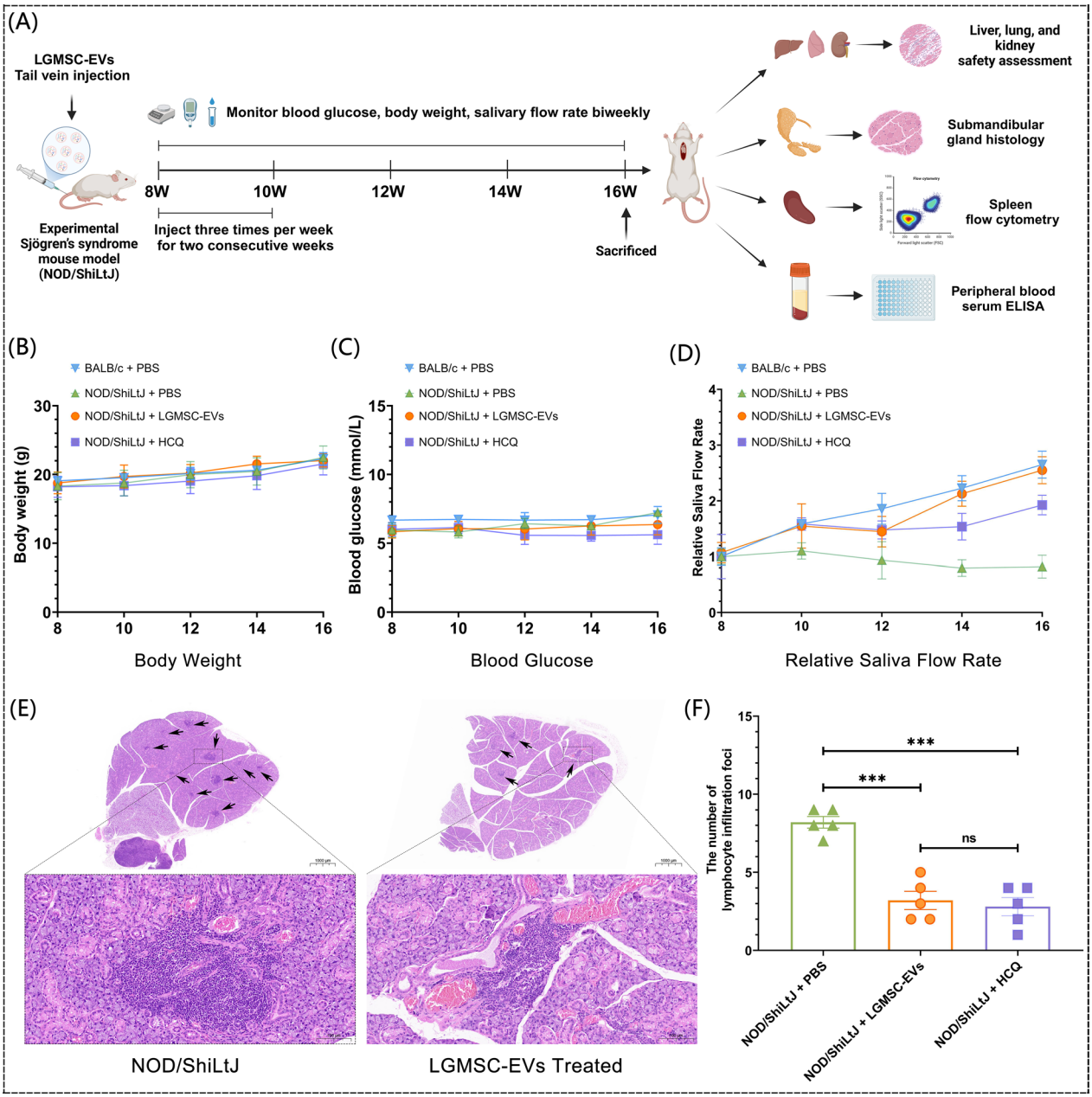

Fig. 2 Therapeutic effects of LGMSC-EVs on experimental SS model. **A** Schematic representation of the experimental design (Created at https://BioRender.com). **B** The body weight of the mice remained stable across all groups throughout the treatment period, showing a steady increase with age (n = 5). **C** Serum glucose levels remained stable across all groups throughout the treatment period (n = 5). **D** Salivary flow rates were significantly increased in the LGMSC-EV-treated group compared to the PBS control group, with effects surpassing those of HCQ treatment after 12 weeks of age (n = 5). **E**–**F** Histopathological analysis of submandibular glands. LGMSC-EV treatment significantly reduced the number and size of lymphocytic infiltration foci, showing comparable efficacy to HCQ treatment (n = 5). A black arrow indicates a lymphocytic infiltration focus (a group of ≥ 50 lymphocytes of gland tissue). Scale bars = 50 μm. *$p < 0.05$, **$p < 0.01$, ***$p < 0.001$, ns: no significance

cytometry-based and target prediction screening of these miRNAs, we identified miRNA let-7f-5p, the fifth most abundant miRNA in LGMSC-EVs, as a potential suppressor of Th17 cells in SS.

To clarify the role of miRNA let-7f-5p in LGMSC-EVs, we transfected LGMSC-EVs with let-7f-5p mimic and let-7f-5p inhibitor to construct miRNA-overexpressing and -knockdown LGMSC-EVs, respectively. The successful transfection of let-7f-5p into LGMSC-EVs was confirmed

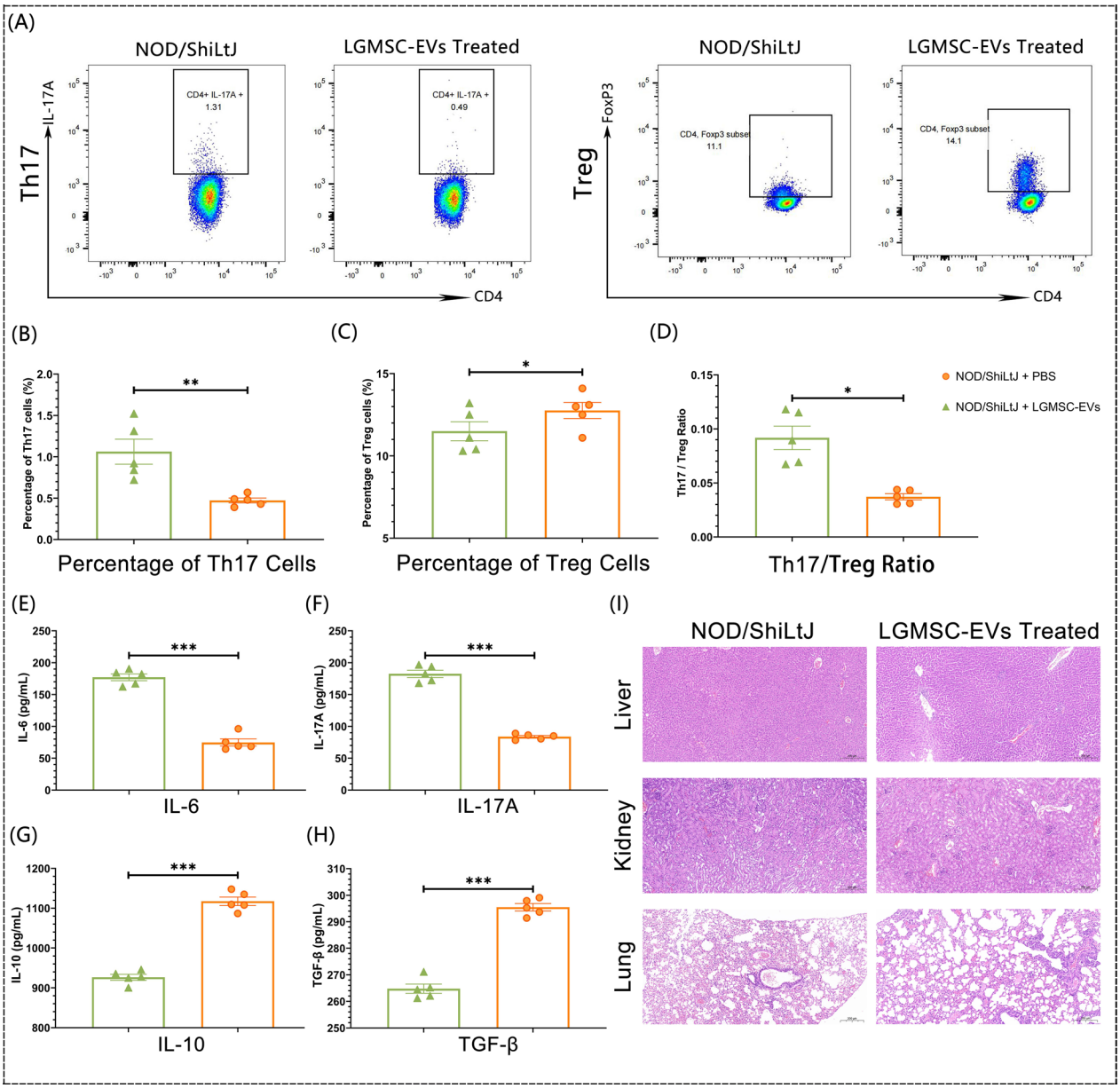

Fig. 3 LGMSC-EVs suppress Th17 cells, modulate the Th17/Treg balance, and demonstrate a favorable safety profile. **A** Flow cytometric analysis of Th17 ($CD4^+IL\text{-}17A^+$) and Treg ($CD4^+Foxp3^+$) cells in the spleens of treated mice (n = 5). **B**–**C** Quantification of the percentage of Th17 and Treg cells. LGMSC-EV treatment significantly reduced the proportion of Th17 cells while modestly increasing the proportion of Treg cells compared to the PBS control group (n = 5). **D** Th17/Treg ratio in the spleens. LGMSC-EV treatment markedly decreased the Th17/Treg ratio compared to the PBS control group (n = 5). **E**–**H** Serum cytokine levels measured by ELISA. LGMSC-EV treatment reduced the levels of IL-6 and IL-17A while increasing the levels of IL-10 and TGF-β compared to PBS controls (n = 5). **I** Safety evaluation of LGMSC-EVs. Histological assessments of liver, kidney, and lung tissues revealed no significant systemic toxicity in treated mice. *$p < 0.05$, **$p < 0.01$, ***$p < 0.001$, *ns* no significance

by qRT-PCR, which showed a significant increase in miRNA let-7f-5p expression, while those transfected with let-7f-5p inhibitor exhibited decreased levels ($p < 0.001$, Fig. 4C). These transfected EVs were then co-cultured with PBMCs isolated from SS patients. The results demonstrated that LGMSC-EVs$^{\text{let-7f-5p mimic}}$ significantly reduced the proportion of Th17 cells and the Th17/Treg ratio in PBMCs, while increasing the proportion of Treg cells. These effects were notably stronger than those of LGMSC-EVs^{NC}. In contrast, LGMSC-EVs$^{\text{let-7f-5p inhibitor}}$ exhibited a marked reduction in their ability to regulate Th17 cells and the Th17/Treg balance (Fig. 4D–G).

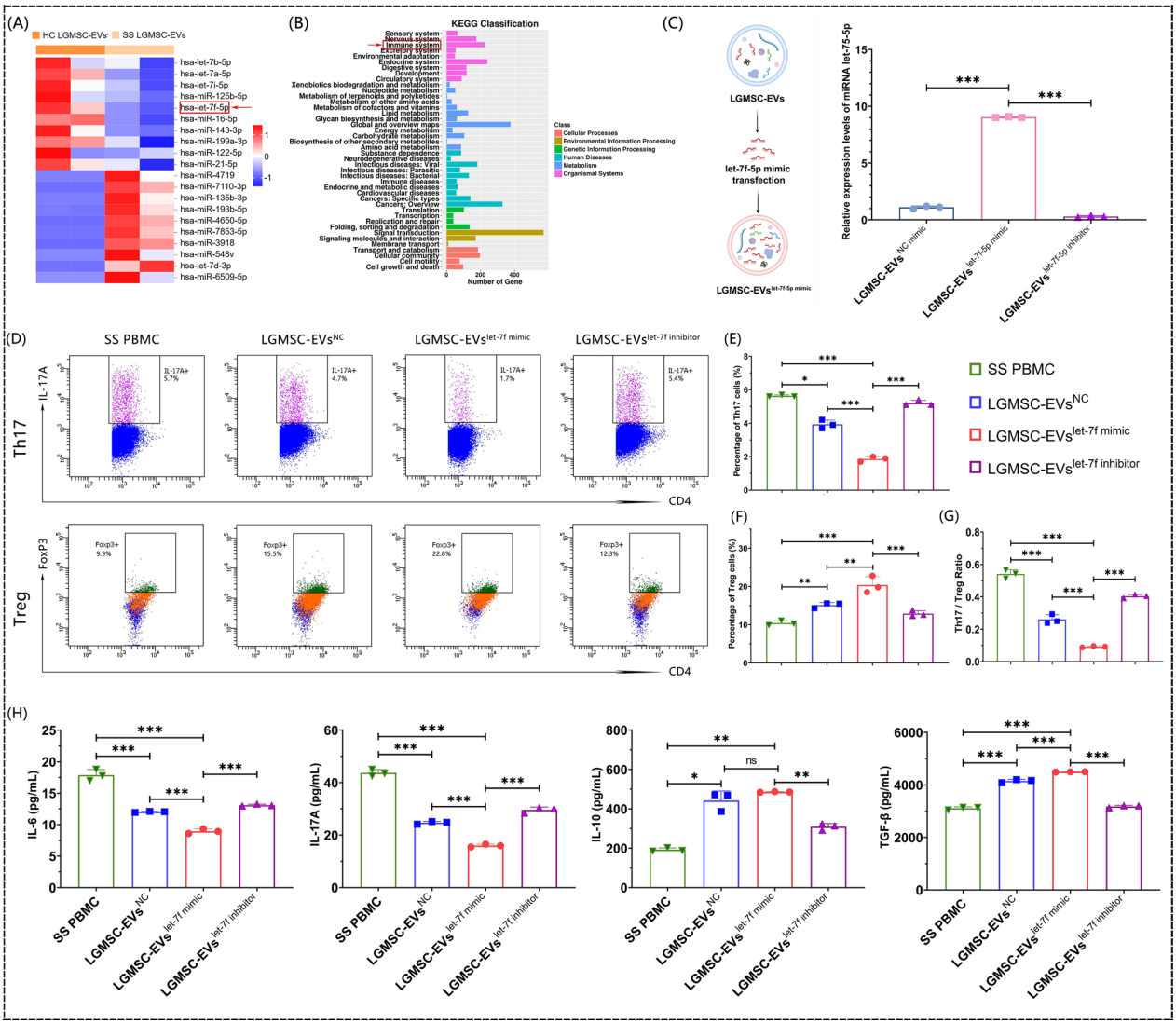

Fig. 4 miRNA let-7f-5p in LGMSC-EVs plays a key role in suppressing Th17 cells and modulating the Th17/Treg balance. **A** The top 10 significantly upregulated miRNAs in LGMSC-EVs derived from HC and SS patients. **B** KEGG pathway classification of predicted gene targets for the upregulated miRNAs from LGMSC-EVs, showing that immune system-related pathways are prominently enriched, ranking second. **C** Schematic representation of the transfection strategy for introducing exogenous miRNA let-7f-5p into LGMSC-EVs using let-7f-5p mimic and inhibitor (left), and qRT-PCR validation of let-7f-5p expression in transfected LGMSC-EVs (right). Expression of let-7f-5p was significantly increased in LGMSC-EVs$^{let-7f\ mimic}$, while it was decreased in LGMSC-EVs$^{let-7f\ inhibitor}$. **D**–**G** Flow cytometry analysis of Th17 ($CD4^+IL\text{-}17A^+$) and Treg ($CD4^+Foxp3^+$) cells in PBMCs from SS patients. LGMSC-EVs$^{let-7f\ mimic}$ significantly reduced the proportion of Th17 cells and the Th17/Treg ratio, while increasing the proportion of Treg cells compared to LGMSC-EVs^{NC}. LGMSC-EVs$^{let-7f\ inhibitor}$ showed diminished regulatory effects. **H** ELISA analysis of cytokines in the supernatants of co-cultured PBMCs. LGMSC-EVs$^{let-7f\ mimic}$ significantly decreased IL-6 and IL-17A levels while increasing IL-10 and TGF-β levels compared to LGMSC-EVs^{NC}. Conversely, LGMSC-EVs$^{let-7f\ inhibitor}$ displayed reduced cytokine modulation effects. The schematic diagrams were created at https://BioRender.com. $^*p < 0.05$, $^{**}p < 0.01$, $^{***}p < 0.001$, ns: no significance

Subsequent ELISA analysis of the supernatants from the co-cultured SS PBMCs revealed that LGMSC-EVs$^{let-7f-5p\ mimic}$ significantly decreased the levels of cytokines IL-6 and IL-17A, while increasing the levels of IL-10 and TGF-β. In contrast, the cytokine modulation effects were diminished in PBMCs treated with LGMSC-EVs$^{let-7f-5p\ inhibitor}$ (Fig. 4H). All these changes were more pronounced than those observed with LGMSC-EVs^{NC}. Therefore, let-7f-5p within LGMSC-EVs plays an essential role in suppressing Th17 cells, thereby modulating the Th17/Treg balance and alleviating inflammatory processes in SS.

let-7f-5p-encapsulated LGMSC-EVs show enhanced efficacy in vivo in alleviating SS symptoms

Based on the in vitro findings, we further constructed let-7f-5p-encapsulated LGMSC-EVs using in vivo-optimized let-7f-5p agomir and antagomir via miRNA transfection (Fig. 5A). The let-7f-5p agomir and antagomir are chemically engineered, stable double-stranded miRNA analogs. These synthetic miRNA molecules are designed to exhibit high stability and improved transfection efficiency, particularly within tissue environments, making them a reliable tool for delivering miRNAs in animal models [41–44]. After transfection, the morphology, particle size, and protein expression of let-7f-5p-encapsulated LGMSC-EVs were then re-evaluated. TEM confirmed their characteristic cup-shaped morphology, NTA revealed an average particle size of 134.7 nm, and western blotting confirmed the presence of exosome markers CD63, CD81, and TSG101, while calnexin was absent, indicating high EV purity (Fig. 5B–D).

We then evaluated the therapeutic effects of let-7f-5p-encapsulated LGMSC-EVs in NOD/ShiLtJ mice (Fig. 5E). Throughout the study, the body weight of the mice increased steadily with age, and their blood glucose levels remained stable (Fig. 5F–H). Importantly, administration of LGMSC-EVs$^{\text{let-7f agomir}}$ significantly enhanced salivary flow rates and reduced both the number and size of lymphocytic infiltration foci in the submandibular glands, demonstrating enhanced efficacy in alleviating SS symptoms compared to LGMSC-EVs$^{\text{NC}}$. In contrast, administering LGMSC-EVs$^{\text{let-7f antagomir}}$ led to decreased salivary flow rates and more extensive lymphocytic infiltration foci in the submandibular glands (Fig. 5I–J), further suggesting that encapsulating LGMSC-EVs with let-7f-5p has the potential to enhance therapeutic efficacy compared to regular LGMSC-EVs. Furthermore, we evaluated the liver, lung, and kidney conditions of NOD/ShiLtJ mice following intravenous injection of let-7f-5p-encapsulated LGMSC-EVs. Histopathological analysis of these organs revealed no evidence of inflammatory cell infiltration or tissue damage (Fig. 5K). These findings suggest that let-7f-5p-encapsulated LGMSC-EVs do not induce severe systemic toxicity and have a favorable safety profile.

let-7f-5p-encapsulated LGMSC-EVs significantly enhance in vivo regulation of Th17/Treg balance, primarily by strengthening Th17 suppression

Following the successful construction of let-7f-5p-encapsulated LGMSC-EVs and the preliminary evaluation of their therapeutic effects on SS mouse model, we sought to confirm whether these EVs exhibit enhanced regulatory effects on the Th17/Treg balance in vivo. Therefore, we evaluated the proportions of Th17 and Treg cells in the spleens of NOD/ShiLtJ mice, along with serum levels of inflammatory cytokines, following intravenous injection as described previously.

The results showed that mice treated with LGMSC-EVs$^{\text{let-7f-5p agomir}}$ exhibited a significant decrease in the proportion of $CD4^+IL\text{-}17A^+$ Th17 cells, with the mean percentage dropping from 1.43% to 0.13% (a 91% reduction, $p = 0.000$), and a marked decrease in the Th17/Treg ratio, from 0.14 to 0.01 (a 93% reduction, $p = 0.000$). Meanwhile, the proportion of $CD4^+Foxp3^+$Treg cells increased from 9.98% to 13.12% ($p = 0.000$) compared to the PBS-treated group (Fig. 6A–D). Cytokine analysis further confirmed these findings, showing significantly reduced levels of IL-6 and IL-17A, alongside elevated levels of IL-10 and TGF-β (Fig. 6E–H). Importantly, the regulatory effects, especially on Th17 suppression and IL-17A reduction, were more significant in the LGMSC-EVs$^{\text{let-7f-5p agomir}}$ group compared to the non-transfected LGMSC-EVs$^{\text{NC}}$ group ($p = 0.000$). Conversely, mice injected with LGMSC-EVs$^{\text{let-7f-5p inhibitor}}$ showed elevated levels of Th17 cells and IL-17A.

Collectively, these findings suggest that let-7f-5p-encapsulated LGMSC-EVs provide more effective modulation of the Th17/Treg balance and cytokine response, primarily through Th17 suppression (Fig. 6I). This highlights their potential therapeutic advantage in restoring Th17/Treg homeostasis and reducing inflammatory responses in the treatment of SS.

(See figure on next page.)

Fig. 5 Construction of let-7f-5p-encapsulated LGMSC-EVs and the in vivo therapeutic evaluation in alleviating SS symptoms. **A** Schematic diagram of the transfection strategy for constructing let-7f-5p-encapsulated LGMSC-EVs using in vivo-optimized let-7f-5p agomir and antagomir. **B**–**D** Characterization of let-7f-5p-encapsulated LGMSC-EVs. **E** Schematic representation of the in vivo experimental design to evaluate the therapeutic effects of let-7f-5p-encapsulated LGMSC-EVs in NOD/ShiLtJ mice. **F**–**H** The body weight and blood glucose levels of the mice remained stable throughout the study in all groups. Administration of LGMSC-EVs$^{\text{let-7f agomir}}$ significantly enhanced the salivary flow rates of the mice compared to LGMSC-EVs$^{\text{NC}}$ (n = 5). **I**–**J** Histopathological analysis of submandibular glands showing reduced lymphocytic infiltration foci in the LGMSC-EVs$^{\text{let-7f agomir}}$ group compared to the control groups (n = 5). A black arrow indicates a lymphocytic infiltration focus (a group of ≥ 50 lymphocytes of gland tissue). Scale bars = 100 μm. **K** Histological analysis of liver, lung, and kidney tissues revealed no signs of tissue damage, indicating that let-7f-5p-encapsulated LGMSC-EVs exhibit a favorable safety profile. The schematic diagrams were created at https://BioRender.com. *$p < 0.05$, **$p < 0.01$, ***$p < 0.001$, *ns* no significance

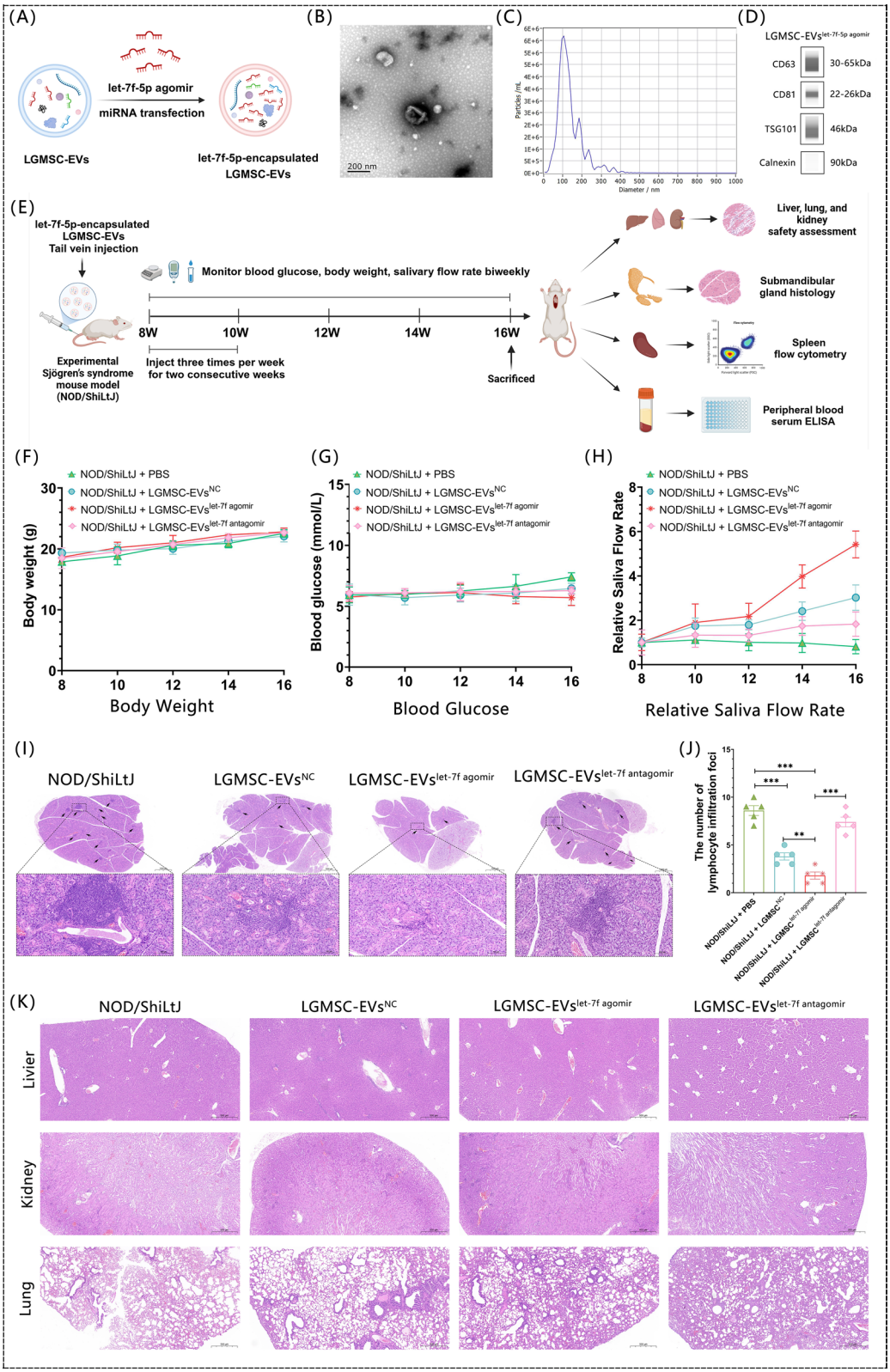

Fig. 5 (See legend on previous page.)

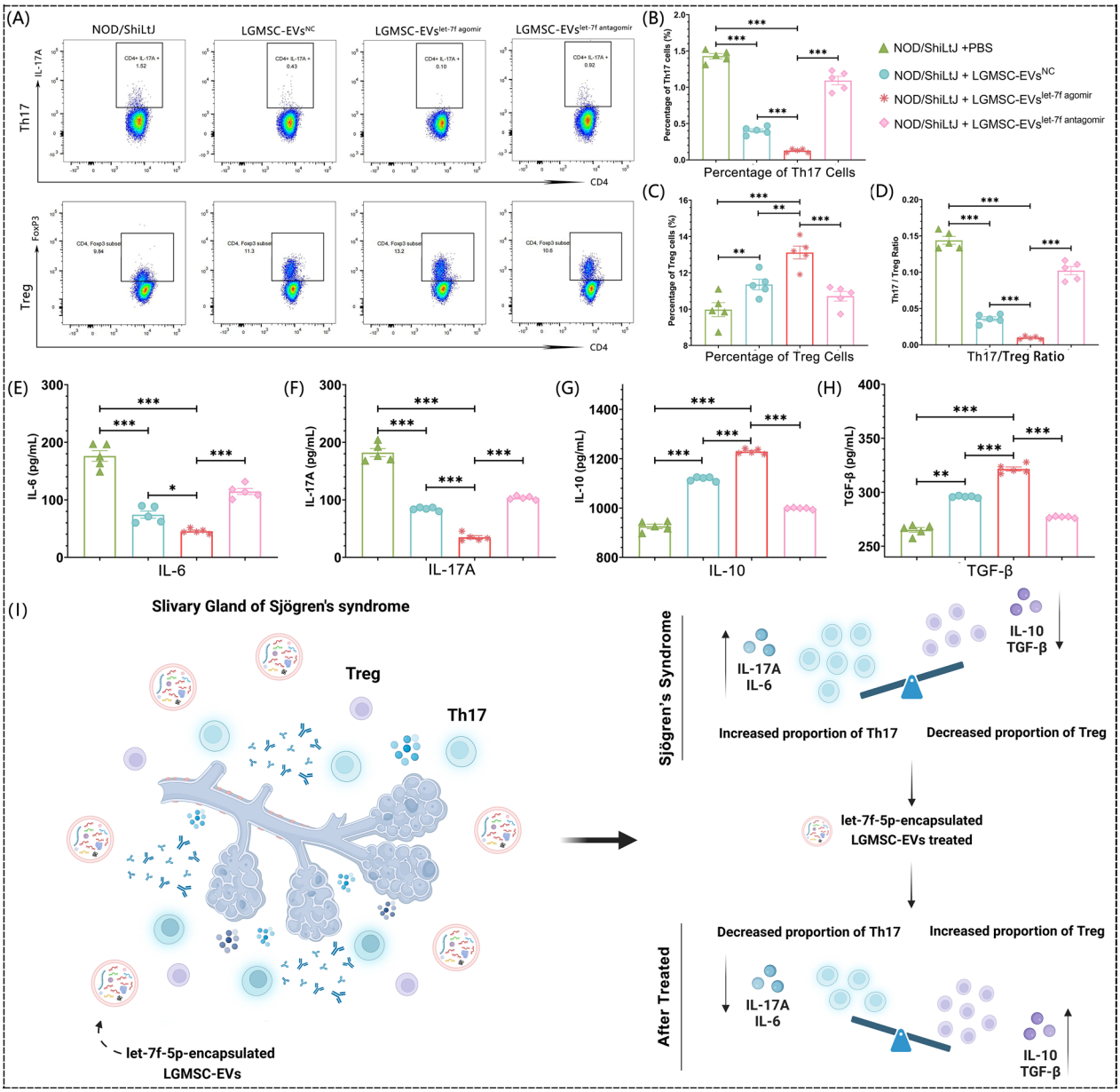

Fig. 6 let-7f-5p-encapsulated LGMSC-EVs significantly enhance the regulation of the Th17/Treg balance in vivo. **A** Representative flow cytometry plots showing $CD4^+IL\text{-}17A^+$ Th17 and $CD4^+Foxp3^+$ Treg cell populations in spleens of NOD/ShiLtJ mice after intravenous injection of PBS, $LGMSC\text{-}EVs^{NC}$, $LGMSC\text{-}EVs^{let-7f-5p\ agomir}$, or $LGMSC\text{-}EVs^{let-7f-5p\ inhibitor}$. **B**–**D** Quantitative analysis of the proportions of $CD4^+IL\text{-}17A^+$ Th17 cells, $CD4^+Foxp3^+$ Treg cells, and the Th17/Treg ratio in the spleen. Mice treated with $LGMSC\text{-}EVs^{let-7f-5p\ agomir}$ exhibited a significant reduction in Th17 cell proportions and Th17/Treg ratio, alongside an increase in Treg cell proportions, compared to PBS and $LGMSC\text{-}EVs^{NC}$ controls. **E**–**H** Serum cytokine analysis showed decreased levels of IL-6 and IL-17A, as well as increased levels of IL-10 and TGF-β in the $LGMSC\text{-}EVs^{let-7f-5p\ agomir}$ group compared to other groups. **I** Schematic diagram illustrating the enhanced regulatory effects of let-7f-5p-encapsulated LGMSC-EVs on the Th17/Treg balance, primarily through suppression of Th17 cells and modulation of cytokine responses. These effects contribute to the restoration of immune homeostasis and improved therapeutic outcomes in the treatment of SS. The schematic diagrams were created at https://BioRender.com. $^*p < 0.05$, $^{**}p < 0.01$, $^{***}p < 0.001$

let-7f-5p-encapsulated LGMSC-EVs suppress Th17 cells by targeting *RORC* and inhibiting *IL-17A* expression

To investigate the molecular mechanism by which let-7f-5p-encapsulated LGMSC-EVs enhance Th17 suppression, we screened target genes of hsa-let-7f-5p and identified *RORC* as a key target, which is an essential transcription factor for Th17 differentiation and IL-17A production [45]. let-7f-5p was predicted to bind

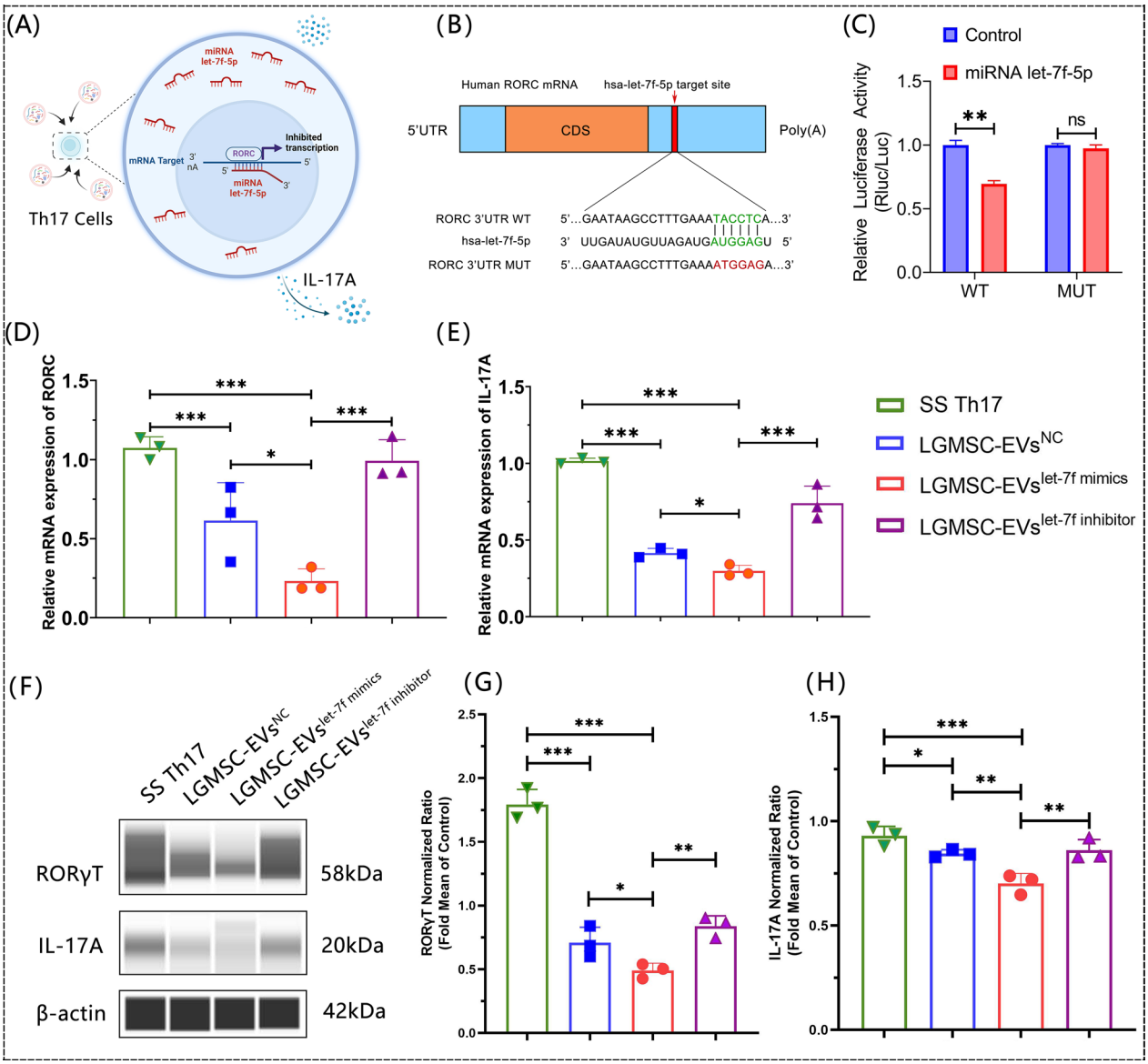

Fig. 7 let-7f-5p-encapsulated LGMSC-EVs suppress Th17 cells by targeting *RORC* and inhibiting *IL-17A* expression. **A** Schematic representation of the mechanism by which let-7f-5p-encapsulated LGMSC-EVs suppress Th17 cells. The released let-7f-5p inhibits *RORC* expression in Th17 cells, thereby suppressing Th17 differentiation and reducing IL-17A production. **B** Schematic model depicting the predicted let-7f-5p binding sites on the 3'UTR of *RORC* (positions 234–239). **C** Dual-luciferase reporter assay demonstrating that let-7f-5p mimic significantly reduces luciferase activity of the WT *RORC* 3'UTR reporter, while no significant reduction was observed in the MUT *RORC* 3'UTR reporter. **D**–**H** qRT-PCR and capillary Western blotting analysis of RORC and IL-17A expression levels in Th17 cells isolated from SS patient PBMCs after co-culture with LGMSC-EVs^{NC}, LGMSC-EVs$^{let-7f-5p\ mimic}$, or LGMSC-EVs$^{let-7f-5p\ inhibitor}$. Th17 cells treated with LGMSC-EVs$^{let-7f-5p\ mimic}$ showed significant downregulation of RORC and IL-17A at both mRNA and protein levels compared to the SS control group and the LGMSC-EVs^{NC} group. The schematic diagrams were created at https://BioRender.com. *$p < 0.05$, **$p < 0.01$, ***$p < 0.001$

to the 3'UTR of *RORC* at positions 234–239, thereby inhibiting its expression (Fig. 7A–B). This interaction was confirmed using dual-luciferase reporter assays. WT and MUT *RORC* 3'UTR luciferase reporter constructs were co-transfected with let-7f-5p mimic into 293 T cells. Co-transfection with the *RORC*-WT construct significantly reduced luciferase activity compared to the *RORC*-MUT construct ($p = 0.002$), confirming that let-7f-5p directly binds to the 3'UTR of *RORC* and inhibits its expression. In contrast, no significant reduction in luciferase activity was observed in the *RORC*-MUT group, verifying that the mutation

disrupted the ability of let-7f-5p to bind and inhibit *RORC* (Fig. 7C).

To validate these findings in vitro, Th17 cells were isolated from SS patient PBMCs using magnetic beads specific for Th17 cells, following co-culture with LGMSC-EVs^{NC}, LGMSC-EVs$^{let-7f-5p\ mimic}$, or LGMSC-EVs$^{let-7f-5p\ inhibitor}$. This approach ensured the isolation of viable Th17 cells, reducing non-specific effects and enhancing sensitivity for downstream analysis. RNA and protein extracted from the isolated Th17 cells were used for qRT-PCR and capillary Western blotting. Th17 cells treated with LGMSC-EVs$^{let-7f-5p\ mimic}$ exhibited a significant downregulation of *RORC* and *IL-17A* at both mRNA and protein levels compared to the SS control group ($p < 0.001$), as well as those treated with LGMSC-EVs^{NC} ($p < 0.05$). Conversely, treatment with LGMSC-EVs$^{let-7f-5p\ inhibitor}$ resulted in *RORC* and *IL-17A* expression levels returning to those observed in untreated Th17 cells from SS patients (Fig. 7D–H).

These findings provide in vitro evidence that let-7f-5p-encapsulated LGMSC-EVs exert therapeutic effects for SS by directly targeting the key transcription factor *RORC* in Th17 cells, suppressing its expression, thereby reducing Th17 cell proportions and decreasing the secretion of IL-17A.

In vivo validation of RORC/IL-17A axis suppression in the submandibular glands in NOD/ShiLtJ mice

The mechanism by which let-7f-5p-encapsulated LGMSC-EVs suppress Th17 cells was further evaluated in vivo using submandibular gland tissues from NOD/ShiLtJ mice. Given the critical role of Th17 cells in forming lymphocytic infiltration foci in SS salivary glands, immunofluorescence and immunohistochemistry analyses were performed to examine Th17 cells co-expressing RORγT and IL-17A within these regions. IF analysis showed a high proportion of Th17 cells co-expressing RORγT and IL-17A in the submandibular glands of PBS-treated NOD/ShiLtJ mice. In contrast, LGMSC-EVs$^{let-7f-5p\ agomir}$-treated mice exhibited a significant reduction in Th17 cells co-expressing RORγT and IL-17A within the infiltration foci compared to the PBS control group (Fig. 8A–B).

These results were further supported by IHC findings, which demonstrated significantly reduced expression levels and immunohistochemical scores of RORγT and IL-17A in LGMSC-EVs$^{let-7f-5p\ agomir}$-treated mice compared to both the PBS control ($p < 0.001$) and non-transfected LGMSC-EVs groups ($p < 0.05$). This indicates that let-7f-5p-encapsulated LGMSC-EVs achieve superior Th17-suppressive effects in vivo, particularly in local salivary gland tissues. Conversely, mice treated with LGMSC-EVs$^{let-7f-5p\ antagomir}$ displayed elevated expression levels of RORγT and IL-17A, indicating a loss of let-7f-5p-mediated regulatory effects (Fig. 8C–E).

In summary, these findings demonstrate that let-7f-5p-encapsulated LGMSC-EVs suppress Th17 cells in vivo by targeting the RORC/IL-17A axis. Moreover, they exhibit significant effects in the salivary glands of NOD/ShiLtJ mice, effectively restoring the Th17/Treg balance and modulating the local immune microenvironment, highlighting their potential as a therapeutic approach for SS.

Discussion

SS remains a clinically challenging autoimmune disease with limited treatment options [1, 4]. It primarily affects salivary and other exocrine glands, leading to symptoms like xerostomia and xerophthalmia, but can also involve multiple organs, significantly increasing morbidity [7, 8]. One of the most serious complications is the markedly elevated risk of lymphoma in SS patients, posing a serious threat to patient health [5, 6, 8]. Current clinical therapies, which primarily focus on symptomatic relief and systemic immunosuppression as outlined in the 2020 EULAR guidelines, have significant limitations [19]. Although glucocorticoids, immunosuppressants, and biologics provide therapeutic benefits, long-term use is associated with significant adverse effects, such as increased susceptibility to infections and organ toxicity [18, 19, 46]. These challenges highlight the pressing need for novel therapeutic strategies that not only modulate immune homeostasis but also effectively suppress inflammation, addressing the underlying mechanisms driving SS progression.

MSCs and their EVs offer a promising alternative to conventional therapies for SS and other autoimmune diseases, particularly due to their ability to modulate immune homeostasis, control inflammation, and regulate the immune microenvironment [22, 24, 47]. They actively modulate both innate and adaptive immune responses through direct cell-to-cell interactions and the secretion of paracrine mediators [31, 48, 49]. Our research team first successfully isolated and characterized LGMSCs and LGMSC-EVs [26–28]. Compared to traditional MSC sources, LGMSCs possess potential advantages due to their easy accessibility, minimal invasiveness, and possible tissue specificity in addressing salivary gland dysfunction. To further evaluate the therapeutic potential of LGMSCs and LGMSC-EVs, we conducted in vivo studies using the NOD/ShiLtJ mice, which are one of the most widely used models for studying SS due to their characteristic clinical features that closely resemble the disease, including chronic lymphocytic infiltration of endocrine and exocrine glands, as well as a pronounced immune

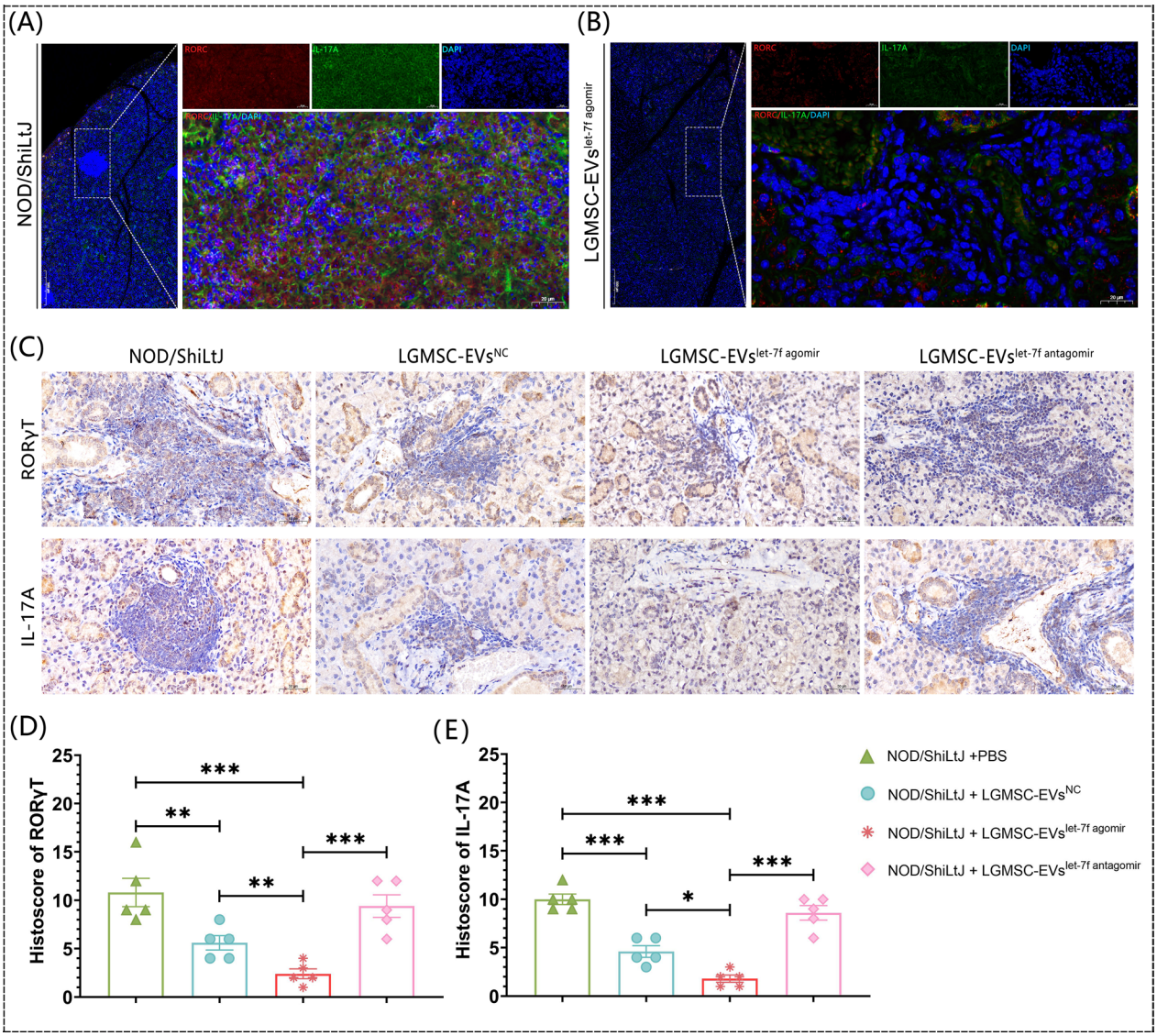

Fig. 8 In vivo suppression of the RORC/IL-17A axis by let-7f-5p-encapsulated LGMSC-EVs in the submandibular glands of NOD/ShiLtJ mice. **A**–**B** IF analysis of submandibular glands from PBS-treated NOD/ShiLtJ mice and those treated with LGMSC-EVs$^{let-7f-5p\ agomir}$. Representative images show Th17 cells co-expressing RORγT (red) and IL-17A (green) within lymphocytic infiltration foci. The proportion of Th17 cells co-expressing RORγT and IL-17A was significantly reduced in the LGMSC-EVs$^{let-7f-5p\ agomir}$-treated group compared to the PBS control group. Scale bars = 20 μm **C**–**E** IHC analysis of RORγT and IL-17A expression in submandibular glands. Representative images show the staining intensity of RORγT and IL-17A in the PBS-treated, LGMSC-EVs^{NC}-treated, LGMSC-EVs$^{let-7f-5p\ agomir}$-treated, and LGMSC-EVs$^{let-7f-5p\ antagomir}$-treated groups (n = 5). Histoscores were calculated by combining two parameters: staining intensity and the percentage of positive cells. The final histoscore was obtained by multiplying these two scores. Quantification of histoscores revealed significantly reduced expression levels in the LGMSC-EVs$^{let-7f-5p\ agomir}$-treated group compared to both the PBS control and non-transfected LGMSC-EVs groups. Scale bars = 50 μm. $^{*}p < 0.05$, $^{**}p < 0.01$, $^{***}p < 0.001$

dysregulation [38–40]. The inflammatory process in the salivary glands begins around 7–8 weeks of age, marking the initial stage, with severe inflammatory lesions becoming evident by 12–16 weeks, during the clinical phase [50, 51]. Corresponding to these infiltrates, a slight reduction in saliva flow is typically observed between 8 and 12 weeks of age, progressing to significantly reduced secretion by 16–24 weeks [50, 51]. Our results demonstrated that intravenous administration of LGMSCs or LGMSC-EVs at 8 weeks of age significantly increased salivary secretion, effectively alleviating xerostomia symptoms by 16 weeks of age in the treated mice. Moreover, histopathological analysis revealed a marked reduction in inflammatory cell infiltration within the submandibular glands. These findings highlight the potential of LGMSCs and their

EVs in mitigating SS symptoms, and prompted further investigation into the underlying immunoregulatory mechanisms, which is critical to the pathogenesis of SS.

Compared to cell-based therapies, EVs, as a natural nano-delivery system, provide a safer and more versatile therapeutic approach, as they minimize risks like tumorigenicity and embolism [30, 31]. Their stability and precision make them ideal candidates for future therapies [25]. Numerous studies have demonstrated the therapeutic potential of EVs in autoimmune diseases through their immunomodulatory capabilities and targeted delivery of therapeutic agents [24]. In rheumatoid arthritis (RA), periarticular injections of EVs have been shown to alleviate arthritis symptoms by delivering anti-inflammatory agents directly to the affected tissues [52]. Additionally, EVs serve as efficient drug carriers, enhancing cartilage penetration and preserving antibody activity, providing a precise therapeutic approach for RA [53]. In systemic lupus erythematosus (SLE), MSC-derived EVs exhibit the ability to cross the blood–brain barrier, making them promising candidates for treating lupus encephalopathy [54, 55]. Moreover, their ease of large-scale production and lower risk of immune reactions further enhance their potential for clinical application in RA and SLE [55]. Moreover, many EV-based therapies have progressed to early-phase clinical trials [56]. Accordingly, the properties of EVs highlight the transformative potential of LGMSC-EVs in offering safer, more precise, and effective therapeutic options in clinical practice for SS and other autoimmune disorders.

miRNAs within EVs have emerged as crucial regulators of immune responses and inflammation, significantly enhancing the therapeutic potential of EV-based therapies [29, 57]. As post-transcriptional regulators, miRNAs modulate gene expression by targeting mRNA, thereby influencing a wide array of cellular processes, including immune cell differentiation, cytokine production, and inflammatory signaling pathways [58]. EVs have been considered an ideal platform for miRNA-based therapies due to their ability to protect miRNAs from RNase-mediated degradation. Therefore, EV-delivered miRNAs have demonstrated substantial potential in the treatment of autoimmune diseases, cancer, and inflammatory disorders, highlighting the development of new clinical interventions.

In recent years, bioengineered EVs have made significant progress in autoimmune disease therapy by precisely modifying their cargo and surface markers [52, 59]. These EVs are typically modified through genetic engineering or chemical approaches, addressing the limitations of natural exosomes. Such modifications enhance their biological activity, stability, and targeting efficiency while improving their specificity and cargo delivery capabilities, making them more effective in facilitating autoimmune disease therapy [60]. Based on these advancements, miRNA-loaded EVs have demonstrated promising therapeutic potential in RA [52]. For instance, miRNA-124 delivered via hybrid micelles co-loaded with methotrexate enhanced anti-inflammatory and bone-protective effects, while PLGA microspheres co-encapsulating miRNA-124 and ketoprofen achieved synergistic outcomes in reducing inflammation and bone damage [61]. Additionally, the combination of miRNA-21 and IL-4, delivered through inflammation-responsive nano complexes, effectively modulated the osteoimmune microenvironment, offering a novel approach for RA therapy [62]. In the treatment of SLE, overexpression of miRNA-155 in MSC-EVs within the CIA model was reported to suppress autoreactive lymphocyte proliferation, enhance the generation of regulatory T cells, and increase anti-inflammatory cytokines like IL-10 [63]. In another study, adipose-derived MSC-EVs loaded with miRNA-10a via electroporation demonstrated the ability to direct naïve T cells toward Th17 and Treg lineages while suppressing differentiation into the Th1 phenotype [64]. However, in SS, research on engineered EVs remains limited, primarily focusing on their potential as diagnostic tools for identifying biomarkers. For instance, a study utilizing nanoporous membrane-based resonators (iTEARS) achieved rapid and efficient isolation of EVs from small volumes of tear fluid, enabling the detection of biomarkers such as miR-145-5p, miR-214-3p, miR-218-5p, and miR-9-5p for ocular diseases [65, 66]. Despite these advancements, therapeutic applications of engineered EVs in SS are still underexplored.

In our study, miRNA sequencing of LGMSC-EVs identified let-7f-5p as the fifth most enriched miRNA, playing an essential role in regulating the Th17/Treg balance in experimental SS, particularly by suppressing Th17 cells, which are key drivers of the inflammatory environment in SS. Then we encapsulated LGMSC-EVs by directly transfecting miRNA let-7f-5p into the EVs via Exo-Fect™ Exosome Transfection Kit, a highly efficient and gentle transfection reagent. Unlike traditional approaches, which require miRNA transfection into cells followed by EV production, Exo-Fect™ enables the direct incorporation of miRNA into pre-isolated EVs, preserving the structural integrity of the EVs and minimizing potential damage associated with more aggressive techniques like electroporation [33, 67–69]. TEM, NTA, and Western blotting confirmed that the LGMSC-EVs retained their typical morphological and molecular characteristics post-transfection, while qRT-PCR validated high transfection efficiency, with elevated

levels of let-7f-5p within the EVs. To further evaluate the therapeutic potential of let-7f-5p-encapsulated LGMSC-EVs, we utilized let-7f-5p agomir, a synthetic mimic optimized for in vivo applications, to overexpress let-7f-5p in LGMSC-EVs. These synthetic miRNA molecules are designed to exhibit high stability and improved transfection efficiency, particularly within tissue environments, making them a reliable tool for delivering miRNAs in animal models [41–44]. In NOD/ShiLtJ mice, these encapsulated EVs significantly improved SS-like symptoms by suppressing Th17 cells and IL-17A expression, thereby rebalancing the Th17/Treg ratio, and restoring immune homeostasis. This suppression led to increased salivary flow rates, and reduced lymphocytic infiltration in the salivary glands, with no signs of systemic toxicity observed. Notably, the therapeutic effects were significantly superior to those observed with non-transfected LGMSC-EVs. Therefore, our study highlights let-7f-5p-encapsulated LGMSC-EVs as a promising therapeutic strategy and provides new insights into the use of engineered EVs for SS treatment.

Furthermore, our findings are supported by evidence that let-7f-5p also plays an essential role in immune regulation in various autoimmune diseases. In multiple sclerosis (MS), let-7f-5p suppresses Th17 differentiation by directly targeting STAT3, a critical transcription factor in Th17 cell development, thus reducing the inflammatory response [70]. In SLE, let-7f-5p attenuates inflammation by downregulating the NLRP3 inflammasome, leading to decreased production of pro-inflammatory cytokines such as IL-1β [71]. In Alzheimer's disease (AD), let-7f-5p enhances the survival of transplanted mesenchymal stem cells [72]. Collectively, these findings highlight the broad regulatory potential of let-7f-5p in immune modulation, reinforcing its therapeutic promise in various autoimmune disorders.

miRNAs have also gained increasing recognition for their critical roles in a wide range of diseases, including cancers, stem cell-related disorders, inflammation, and other pathological conditions. Among them, miR-21 has been identified as a significant biomarker and potential therapeutic target due to its involvement in various cellular processes [73]. In myeloid leukemia, miR-21 is consistently upregulated, suggesting its contribution to cancer progression. Inhibition of miR-21 has shown promising results in reducing cell proliferation and inducing apoptosis in leukemia cell lines and mouse models. Interestingly, miR-21 is upregulated in myelodysplastic syndrome and chronic myeloid leukemia, while its expression is downregulated in certain subtypes of acute myeloid leukemia, highlighting the complexity of its role across different leukemia subtypes. In addition to its involvement in cancer, miR-21 also plays a significant role in MSC differentiation [74]. Its upregulation facilitates MSC differentiation into osteoblasts and adipocytes, while downregulation impedes this process, though further research is required to fully understand its impact on chondrogenesis. Furthermore, recent studies have revealed that two novel miRNAs, miR-24 and miR-466i, are upregulated in rat hepatocytes in response to inflammatory stimuli, indicating their potential as therapeutic targets for liver injury [75]. These findings underscore the multifaceted roles of miR-21, miR-24, miR-466i and other related miRNAs in disease pathogenesis, particularly in cancers, stem cell biology, and inflammation. The intricate regulatory mechanisms of these miRNAs underscore their therapeutic potential across diverse diseases, highlighting the significance of exploring their molecular mechanisms.

In terms of mechanisms, we used multiple miRNA databases for target prediction and identified *RORC* as a key target of let-7f-5p, which is a key transcription factor for Th17 differentiation for Th17 differentiation. Dual-luciferase reporter assays further confirmed that let-7f-5p directly binds to the 3'UTR of *RORC* in Th17 cells. Th17 cells, particularly through IL-17A production, play a central role in SS pathogenesis by initiating autoimmune epithelitis, sustaining chronic inflammation, and contributing to ectopic germinal center (GC) formation [13]. The regulation of the RORC/IL-17A axis is critical, as IL-17A not only links T- and B-cell compartments but also drives GC formation, which perpetuates autoantibody production and accelerates disease progression [37, 76]. Reducing IL-17A levels may disrupt these pathological processes and alleviate SS symptoms [77]. Therefore, early inhibition of Th17 cell activation can effectively disrupt the cascade of pathological events, including excessive B cell activation and pro-inflammatory cytokine release, thereby reducing immune-mediated glandular damage and slowing SS progression [78].

In this study, Th17 cells were further isolated from SS patient PBMCs using magnetic bead sorting, and analysis using qRT-PCR and Western blotting demonstrated significant downregulation of both RORC and IL-17A in Th17 cells treated with let-7f-5p-encapsulated EVs. These findings were further substantiated through in vivo experiments using immunohistochemistry and immunofluorescence. Additionally, our findings showed a notable cytokine shift, characterized by the suppression of IL-6 and the upregulation of TGF-β and IL-10. IL-6 is essential for maintaining the transcriptional and functional identity of Th17 cells through continuous classical receptor signaling, thus promoting inflammatory responses in SS [79]. Conversely, TGF-β promotes the development of Tregs by regulating the expression of

Foxp3, a key transcription factor for Treg differentiation [80]. Additionally, IL-10 production can suppress the Tfh cell response, thereby mitigating the progression of SS [81]. Therefore, by promoting this cytokine shift, let-7f-5p-encapsulated EVs suppress inflammatory responses, particularly by reducing Th17-driven inflammation, which perpetuates immune dysregulation in SS.

Significant advancements have also been made in developing therapies targeting Th17/IL-17-related pathways for autoimmune diseases, with multiple clinical trials underway [17]. For instance, Bimekizumab, the first bispecific antibody approved by the FDA in 2021, selectively inhibits both IL-17A and IL-17F [82]. It has demonstrated comparable efficacy to adalimumab in reducing symptoms of plaque psoriasis and has also shown promising results in clinical trials for moderate-to-severe plaque psoriasis, rheumatoid arthritis, and ankylosing spondylitis[83–85]. Despite these advancements, no clinical trials targeting Th17/IL-17 pathways have been conducted for SS. Therefore, our study provides a novel perspective for the future clinical translation of Th17/IL-17-targeted therapies in SS.

Collectively, this study presents an innovative approach by encapsulating LGMSC-EVs with miRNA let-7f-5p, specifically targeting the RORC/IL-17A axis to modulate the Th17/Treg balance, a critical mechanism in SS pathogenesis. By identifying let-7f-5p as a key regulatory miRNA within LGMSC-EVs, we have developed a molecular-targeted, mechanism-based strategy for immune modulation in SS. These results underscore the therapeutic potential of encapsulated EVs, positioning them as a promising next-generation platform for SS treatment. In future studies, validating the therapeutic efficacy and safety of let-7f-5p-encapsulated LGMSC-EVs in more advanced preclinical models, such as non-human primates, will be essential for facilitating translation of this approach to clinical applications.

Conclusion

This study presents a novel therapeutic strategy using let-7f-5p-encapsulated LGMSC-EVs to target the RORC/IL-17A axis, which plays a critical role in SS pathogenesis. By restoring the Th17/Treg balance, these encapsulated EVs showed effective therapeutic efficacy without causing systemic toxicity. This miRNA let-7f-5p-enhanced LGMSC-EV therapy offers a target-driven and mechanism-based approach to regulate immune responses, making it a promising potential treatment for SS.

Abbreviations

AD	Alzheimer's disease
ELISA	Enzyme-linked immunosorbent assay
EVs	Extracellular vesicles
GC	Germinal center
GO	Gene ontology
HC	Healthy control
HCQ	Hydroxychloroquine
IF	Immunofluorescence
IHC	Immunohistochemistry
IL-17A	Interleukin-17A
KEGG	Kyoto Encyclopedia of Genes and Genomes
LGMSCs	Labial gland mesenchymal stem cells
LGMSC-EVs	Labial gland mesenchymal stem cell derived EVs
miRNA	MicroRNA
MS	Multiple sclerosis
MSCs	Mesenchymal stem cells
MUT	Mutant
NTA	Nanoparticle tracking analysis
qRT-PCR	Quantitative real-time PCR
RA	Rheumatoid arthritis
SLE	Systemic lupus erythematosus
SS	Sjögren's syndrome
TEM	Transmission electron microscopy
UTR	Untranslated region
WT	Wild-type

Supplementary Information

The online version contains supplementary material available at https://doi.org/10.1186/s12951-025-03308-y.

Supplementary material 1
Supplementary material 2
Supplementary material 3
Supplementary material 4
Supplementary material 5

Acknowledgements

We would like to thank Home for Researchers (www.home-for-researchers.com) for English language editing.

Author contributions

YFX: Conceptualization, Methodology, Formal analysis, Investigation, Writing-original draft; MSC: Methodology, Investigation; YXX: Methodology, Formal analysis; PRZ: Writing-review & editing, Funding acquisition, Project administration; Supervision; PW: Project administration, Supervision, Resources; HH: Writing-review & editing, Funding acquisition, Project administration, Supervision, Resources.

Funding

This work was supported by grants from the National Natural Science Foundation of China (grant number 81970952), the Program of New Clinical Techniques of Peking University School and Hospital of Stomatology (PKUSSNCT-24A10), and the Beijing Natural Science Foundation (grant number 7204331).

Data availability

The datasets utilized and analyzed in this study are accessible from the corresponding author upon reasonable request.

Declarations

Ethics approval and consent to participate

The protocol for collecting human labial gland tissues and peripheral blood was reviewed and approved by the Ethics Committee of the Peking University School and Hospital of Stomatology, Beijing, China (Approval No. PKUSSIRB-202498061). The animal care and experimental procedures were approved by the Institutional Animal Care and Use Committee (IACUC) of Peking University Health Science Center, Beijing, China (Approval No. DLASBD0218).

Consent for publication
All authors agree with the publication.

Competing interests
The authors declare no competing interests.

Author details
[1]Department of Oral Medicine, Peking University School and Hospital of Stomatology & National Center for Stomatology & National Clinical Research Center for Oral Diseases & National Engineering Research Center of Oral Biomaterials and Digital Medical Devices, Beijing, China. [2]Department of Stomatology, Zhongshan Hospital, Fudan University, Shanghai, China.

Received: 10 December 2024 Accepted: 8 March 2025
Published online: 20 March 2025

References

1. Brito-Zerón P, Baldini C, Bootsma H, Bowman SJ, Jonsson R, Mariette X, Sivils K, Theander E, Tzioufas A, Ramos-Casals M. Sjögren syndrome. Nat Rev Dis Primers. 2016;2:16047.
2. Beydon M, McCoy S, Nguyen Y, Sumida T, Mariette X, Seror R. Epidemiology of Sjögren syndrome. Nat Rev Rheumatol. 2024;20:158–69.
3. Zhang W, Chen Z, Li X, Gao J, Zhao Y. Recommendations of diagnosis and treatment of primary Sjögren syndrome in China. Chin J Int Med. 2023;62:1059–67.
4. Mariette X, Criswell LA. Primary Sjögren's syndrome. N Engl J Med. 2018;378:931–9.
5. Kapsogeorgou EK, Voulgarelis M, Tzioufas AG. Predictive markers of lymphomagenesis in Sjögren's syndrome: from clinical data to molecular stratification. J Autoimmun. 2019;104:102316.
6. Wu T, Li S, Chen J, Liao J, Huang Z, Yang J, Zhang Y, He Q, Yu X, Song W, et al. A bibliometric analysis of primary Sjögren's syndrome-associated lymphoma from 1991 to 2022. Heliyon. 2023;9:e21337.
7. Zhou Z, Liu H, Yang Y, Zhou J, Zhao L, Chen H, Fei Y, Zhang W, Li M, Zhao Y, et al. The five major autoimmune diseases increase the risk of cancer: epidemiological data from a large-scale cohort study in China. Cancer Commun. 2022;42:435–46.
8. Thorlacius GE, Björk A, Wahren-Herlenius M. Genetics and epigenetics of primary Sjögren syndrome: implications for future therapies. Nat Rev Rheumatol. 2023;19:288–306.
9. Yao Y, Ma J, Chang C, Xu T, Gao C, Gershwin ME, Lian Z. Immunobiology of T cells in Sjögren's syndrome. Clin Rev Allergy Immunol. 2021;60:111–31.
10. Zhan Q, Zhang J, Lin Y, Chen W, Fan X, Zhang D. Pathogenesis and treatment of Sjogren's syndrome: review and update. Front Immunol. 2023;14:1127417.
11. Lin X, Rui K, Deng J, Tian J, Wang X, Wang S, Ko KH, Jiao Z, Chan VS, Lau CS, et al. Th17 cells play a critical role in the development of experimental Sjögren's syndrome. Ann Rheum Dis. 2015;74:1302–10.
12. Cong X, Zhang X, Zhang Y, Wei T, He Q, Zhang L, Hua H, Lee SW, Park K, Yu G, et al. Disruption of endothelial barrier function is linked with hyposecretion and lymphocytic infiltration in salivary glands of Sjögren's syndrome. Biochim Biophys Acta Mol Basis Dis. 2018;1864:3154–63.
13. Verstappen GM, Corneth OBJ, Bootsma H, Kroese FGM. Th17 cells in primary Sjögren's syndrome: Pathogenicity and plasticity. J Autoimmun. 2018;87:16–25.
14. Ming B, Zhu Y, Zhong J, Dong L. Regulatory T cells: a new therapeutic link for Sjögren syndrome? Rheumatology. 2023;62:2963–70.
15. Blinova VG, Vasilyev VI, Rodionova EB, Zhdanov DD. The role of regulatory T cells in the onset and progression of primary Sjögren's syndrome. Cells. 2023.
16. Alunno A, Carubbi F, Bistoni O, Caterbi S, Bartoloni E, Mirabelli G, Cannarile F, Cipriani P, Giacomelli R, Gerli R. T Regulatory and T helper 17 cells in primary Sjögren's syndrome: facts and perspectives. Mediators Inflamm. 2015;2015:243723.
17. Song Y, Li J, Wu Y. Evolving understanding of autoimmune mechanisms and new therapeutic strategies of autoimmune disorders. Signal Transduct Target Ther. 2024;9:263.
18. Gandolfo S, Bombardieri M, Pers JO, Mariette X, Ciccia F. Precision medicine in Sjögren's disease. Lancet Rheumatol. 2024;6:e636–47.
19. Ramos-Casals M, Brito-Zerón P, Bombardieri S, Bootsma H, De Vita S, Dörner T, Fisher BA, Gottenberg JE, Hernandez-Molina G, Kocher A, et al. EULAR recommendations for the management of Sjögren's syndrome with topical and systemic therapies. Ann Rheum Dis. 2020;79:3–18.
20. The Rheumatology Branch of the Chinese Medical Association. Clinical practice guidelines for the treatment of primary Sjögren syndrome by off-label drug use in China. Natl Med J China. 2023;103:3445–61.
21. Wang S, Zhang L, Wei P, Hua H. Is hydroxychloroquine effective in treating primary Sjogren's syndrome: a systematic review and meta-analysis. BMC Musculoskelet Disord. 2017;18:186.
22. Zaripova LN, Midgley A, Christmas SE, Beresford MW, Pain C, Baildam EM, Oldershaw RA. Mesenchymal stem cells in the pathogenesis and therapy of autoimmune and autoinflammatory diseases. Int J Mol Sci. 2023;24:16040.
23. Pharoun J, Berro J, Sobh J, Abou-Younes MM, Nasr L, Majed A, Khalil A, Joseph, Stephan, Faour WH. Mesenchymal stem cells biological and biotechnological advances: Implications for clinical applications. Eur J Pharmacol. 2024;977:176719.
24. Xu K, Liu Q, Wu K, Liu L, Zhao M, Yang H, Wang X, Wang W. Extracellular vesicles as potential biomarkers and therapeutic approaches in autoimmune diseases. J Transl Med. 2020;18:432.
25. Che Shaffi S, Hairuddin ON, Mansor SF, Syafiq TMF, Yahaya BH. Unlocking the potential of extracellular vesicles as the next generation therapy. Tissue Eng Regen Med. 2024;21(513):527.
26. Wang S, Wang Y, Hua H. Characteristics of labial gland mesenchymal stem cells of healthy individuals and patients with Sjögren's syndrome: a preliminary study. Stem Cells Dev. 2017;26:1171–85.
27. Li B, Xing Y, Gan Y, He J, Hua H. Labial gland-derived mesenchymal stem cells and their exosomes ameliorate murine Sjögren's syndrome by modulating the balance of Treg and Th17 cells. Stem Cell Res Ther. 2021;12:478.
28. Xing Y, Li B, He J, Hua H. Labial gland mesenchymal stem cell derived exosomes-mediated miRNA-125b attenuates experimental Sjogren's syndrome by targeting PRDM1 and suppressing plasma cells. Front Immunol. 2022;13: 871096.
29. Vaka R, Parent S, Risha Y, Khan S, Courtman D, Stewart DJ, Davis DR. Extracellular vesicle microRNA and protein cargo profiling in three clinical-grade stem cell products reveals key functional pathways. Mol Ther Nucleic Acids. 2023;32:80–93.
30. Kumar MA, Baba SK, Sadida HQ, Marzooqi SA, Jerobin J, Altemani FH, Algehainy N, Alanazi MA, Abou-Samra AB, Kumar R, et al. Extracellular vesicles as tools and targets in therapy for diseases. Signal Transduct Target Ther. 2024;9:27.
31. Turpin D, Truchetet ME, Faustin B, Augusto JF, Contin-Bordes C, Brisson A, Blanco P, Duffau P. Role of extracellular vesicles in autoimmune diseases. Autoimmun Rev. 2016;15:174–83.
32. Nguyen U, Squaglia N, Boge A, Fung PA. The simple Western™: a gel-free, blot-free, hands-free Western blotting reinvention. Nat Methods. 2011;8:v–vi.
33. de Abreu RC, Ramos CV, Becher C, Lino M, Jesus C, da Costa Martins PA, Martins PAT, Moreno MJ, Fernandes H, Ferreira L. Exogenous loading of miRNAs into small extracellular vesicles. J Extracell Vesicles. 2021;10:e12111.
34. Liu R, Zhang Y, Li K, Xu H, Cheng Z, Pang F, Wu H, Guo Z, He J, Tang X, et al. Effect of acupuncture on regulating IL-17, TNF-α and AQPs in Sjögren's syndrome. Oral Dis. 2024;30:50–62.
35. Chu W, Ding C, Du Z, Wei P, Wang Y, Ge X, Yu G. SHED-exos promote saliva secretion by suppressing p-ERK1/2-mediated apoptosis in glandular cells. Oral Dis. 2024;30:3066–80.
36. Scardina GA, Spanó G, Carini F, Spicola M, Valenza V, Messina P, Maresi E. Diagnostic evaluation of serial sections of labial salivary gland biopsies in Sjögren's syndrome. Med Oral Patol Oral Cir Bucal. 2007;12:E565-568.
37. Xiao F, Lin X, Tian J, Wang X, Chen Q, Rui K, Ma J, Wang S, Wang Q, Wang X, et al. Proteasome inhibition suppresses Th17 cell generation and ameliorates autoimmune development in experimental Sjögren's syndrome. Cell Mol Immunol. 2017;14:924–34.
38. Xiao F, Han M, Wang X, Gong X, Huang E, Zhu Z, Zhao F, Zhao Y, Jiang Q, Lu L. Animal models of Sjögren's syndrome: an update. Clin Exp Rheumatol. 2019;37(Suppl 118):209–16.

39. Du Z, Ding C, Zhang Q, Zhang Y, Ge X, Li S, Yu G. Stem cells from exfoliated deciduous teeth alleviate hyposalivation caused by Sjögren syndrome. Oral Dis. 2019;25:1530–44.
40. Humphreys-Beher MG, Hu Y, Nakagawa Y, Wang PL, Purushotham KR. Utilization of the non-obese diabetic (NOD) mouse as an animal model for the study of secondary Sjögren's syndrome. Adv Exp Med Biol. 1994;350:631–6.
41. Gao L, Qiu F, Cao H, Li H, Dai G, Ma T, Gong Y, Luo W, Zhu D, Qiu Z, et al. Therapeutic delivery of microRNA-125a-5p oligonucleotides improves recovery from myocardial ischemia/reperfusion injury in mice and swine. Theranostics. 2023;13:685–703.
42. Yang F, Chen Q, He S, Yang M, Maguire EM, An W, Afzal TA, Luong LA, Zhang L, Xiao Q. miR-22 Is a novel mediator of vascular smooth muscle cell phenotypic modulation and neointima formation. Circulation. 2018;137:1824–41.
43. Yin H, Wang H, Li Z, Shu D, Guo P. RNA micelles for the systemic delivery of anti-miRNA for cancer targeting and inhibition without ligand. ACS Nano. 2019;13:706–17.
44. Chen W, Chen H, Zheng D, Zhang H, Deng L, Cui W, Zhang Y, Santos HA, Shen H. Gene-hydrogel microenvironment regulates extracellular matrix metabolism balance in nucleus pulposus. Adv Sci. 2020;7:1902099.
45. Capone A, Volpe E. Transcriptional regulators of T helper 17 cell differentiation in health and autoimmune diseases. Front Immunol. 2020;11:348.
46. Baldini C, Fulvio G, La Rocca G, Ferro F. Update on the pathophysiology and treatment of primary Sjögren syndrome. Nat Rev Rheumatol. 2024;20:473–91.
47. Jasim SA, Yumashev AV, Abdelbasset WK, Margiana R, Markov A, Suksatan W, Pineda B, Thangavelu L, Ahmadi SH. Shining the light on clinical application of mesenchymal stem cell therapy in autoimmune diseases. Stem Cell Res Ther. 2022;13:101.
48. Benvenuto F, Voci A, Carminati E, Gualandi F, Mancardi G, Uccelli A, Vergani L. Human mesenchymal stem cells target adhesion molecules and receptors involved in T cell extravasation. Stem Cell Res Ther. 2015;6:245.
49. Gerdoni E, Gallo B, Casazza S, Musio S, Bonanni I, Pedemonte E, Mantegazza R, Frassoni F, Mancardi G, Pedotti R, et al. Mesenchymal stem cells effectively modulate pathogenic immune response in experimental autoimmune encephalomyelitis. Ann Neurol. 2007;61:219–27.
50. Yamano S, Atkinson JC, Baum BJ, Fox PC. Salivary gland cytokine expression in NOD and normal BALB/c mice. Clin Immunol. 1999;92:265–75.
51. Su Y, Xiang R, Zhang Y, Ding C, Cong X, Guo X, Yang N, Hua H, Wu L, Yu G. Decreased submandibular adiponectin is involved in the progression of autoimmune sialoadenitis in non-obese diabetic mice. Oral Dis. 2014;20:744–55.
52. Ren S, Xu Y, Dong X, Mu Q, Chen X, Yu Y, Su G. Nanotechnology-empowered combination therapy for rheumatoid arthritis: principles, strategies, and challenges. J Nanobiotechnology. 2024;22:431.
53. Jouybari MT, Mojtahedi F, Babaahmadi M, Faeed M, Eslaminejad MB, Taghiyar L. Advancements in extracellular vesicle targeted therapies for rheumatoid arthritis: insights into cellular origins, current perspectives, and emerging challenges. Stem Cell Res Ther. 2024;15:276.
54. Fei Y, Liu Q, Peng N, Yang G, Shen Z, Hong P, Wang S, Rui K, Cui D. Exosomes as crucial players in pathogenesis of systemic *Lupus Erythematosus*. J Immunol Res. 2022;2022:8286498.
55. Zhang B, Zhao M, Lu Q. Extracellular vesicles in rheumatoid arthritis and systemic lupus erythematosus: functions and applications. Front Immunol. 2020;11: 575712.
56. Mizenko RR, Feaver M, Bozkurt BT, Lowe N, Nguyen B, Huang KW, Wang A, Carney RP. A critical systematic review of extracellular vesicle clinical trials. J Extracell Vesicles. 2024;13:e12510.
57. Aswani BS, Hegde M, Vishwa R, Alqahtani MS, Abbas M, Almubarak HA, Sethi G, Kunnumakkara AB. Tackling exosome and nuclear receptor interaction: an emerging paradigm in the treatment of chronic diseases. Mil Med Res. 2024;11:67.
58. Chen LL, Kim VN. Small and long non-coding RNAs: past, present, and future. Cell. 2024;187:6451–85.
59. Ji Y, Mi L, Zhao M, He X, Hu Y, Gao Y, Yin C, Xu K. Innovative diagnosis and therapeutic modalities: engineered exosomes in autoimmune disease. Int J Nanomedicine. 2024;19:3943–56.
60. Dooley K, McConnell RE, Xu K, Lewis ND, Haupt S, Youniss MR, Martin S, Sia CL, McCoy C, Moniz RJ, et al. A versatile platform for generating engineered extracellular vesicles with defined therapeutic properties. Mol Ther. 2021;29:1729–43.
61. Yu C, Zhang X, Sun X, Long C, Sun F, Liu J, Li X, Lee RJ, Liu N, Li Y, et al. Ketoprofen and MicroRNA-124 Co-loaded poly (lactic-co-glycolic acid) microspheres inhibit progression of adjuvant-induced arthritis in rats. Int J Pharm. 2018;552:148–53.
62. Deng Y, Zhou Y, Liang Q, Ge C, Yang J, Shan B, Liu Y, Zhou X, Yin L. Inflammation-instructed hierarchical delivery of IL-4/miR-21 orchestrates osteoimmune microenvironment toward the treatment of rheumatoid arthritis. Adv Func Mater. 2021;31:2101033.
63. Yang C, Sun J, Tian Y, Li H, Zhang L, Yang J, Wang J, Zhang J, Yan S, Xu D. Immunomodulatory effect of MSCs and MSCs-derived extracellular vesicles in systemic lupus erythematosus. Front Immunol. 2021;12:714832.
64. Bolandi Z, Mokhberian N, Eftekhary M, Sharifi K, Soudi S, Ghanbarian H, Hashemi SM. Adipose derived mesenchymal stem cell exosomes loaded with miR-10a promote the differentiation of Th17 and Treg from naive CD4(+) T cell. Life Sci. 2020;259:118218.
65. Hu L, Zhang T, Ma H, Pan Y, Wang S, Liu X, Dai X, Zheng Y, Lee LP, Liu F. Discovering the secret of diseases by incorporated tear exosomes analysis via rapid-isolation system: iTEARS. ACS Nano. 2022;16:11720–32.
66. Kim YJ, Yeon Y, Lee WJ, Shin YU, Cho H, Sung YK, Kim DR, Lim HW, Kang MH. Comparison of MicroRNA expression in tears of normal subjects and Sjögren syndrome patients. Invest Ophthalmol Vis Sci. 2019;60:4889–95.
67. Haque S, Vaiselbuh SR. Silencing of Exosomal miR-181a Reverses Pediatric Acute Lymphocytic Leukemia Cell Proliferation. Pharmaceuticals (Basel). 2020;13:27066.
68. Khalyfa A, Kheirandish-Gozal L, Khalyfa AA, Philby MF, Alonso-Álvarez ML, Mohammadi M, Bhattacharjee R, Terán-Santos J, Huang L, Andrade J, et al. Circulating plasma extracellular microvesicle microRNA cargo and endothelial dysfunction in children with obstructive sleep apnea. Am J Respir Crit Care Med. 2016;194:1116–26.
69. Liao K, Niu F, Hu G, Yang L, Dallon B, Villarreal D, Buch S. Morphine-mediated release of miR-138 in astrocyte-derived extracellular vesicles promotes microglial activation. J Extracell Vesicles. 2020;10:e12027.
70. Li Z, Wang Y, He D, Zhang X, Zhou Y, Yue H, Huang S, Fu Z, Zhang L, Mao Z, et al. Let-7f-5p suppresses Th17 differentiation via targeting STAT3 in multiple sclerosis. Aging. 2019;11:4463–77.
71. Tan W, Gu Z, Leng J, Zou X, Chen H, Min F, Zhou W, Zhang L, Li G. Let-7f-5p ameliorates inflammation by targeting NLRP3 in bone marrow-derived mesenchymal stem cells in patients with systemic lupus erythematosus. Biomed Pharmacother. 2019;118:109313.
72. Han L, Zhou Y, Zhang R, Wu K, Lu Y, Li Y, Duan R, Yao Y, Zhu D, Jia Y. MicroRNA Let-7f-5p promotes bone marrow mesenchymal stem cells survival by targeting caspase-3 in Alzheimer disease model. Front Neurosci. 2018;12:333.
73. Panagal M, S R SK, P S, M B, M K, Gopinathe V, Sivakumare P, Sekar D. MicroRNA21 and the various types of myeloid leukemia. Cancer Gene Ther. 2018;25:161–6.
74. Sekar D, Saravanan S, Karikalan K, Thirugnanasambantham K, Lalitha P, Islam VI. Role of microRNA 21 in mesenchymal stem cell (MSC) differentiation: a powerful biomarker in MSCs derived cells. Curr Pharm Biotechnol. 2015;16:43–8.
75. Saravanan S, Thirugnanasambantham K, Hanieh H, Karikalan K, Sekar D, Rajagopalan R, Hairul Islam VI. miRNA-24 and miRNA-466i-5p controls inflammation in rat hepatocytes. Cell Mol Immunol. 2015;12:113–5.
76. Xiao F, Rui K, Han M, Zou L, Huang E, Tian J, Zhang L, Jiang Q, Wu Y, Lu L. Artesunate suppresses Th17 response via inhibiting IRF4-mediated glycolysis and ameliorates Sjo̊gren's syndrome. Signal Transduct Target Ther. 2022;7:274.
77. Xiao F, Du W, Zhu X, Tang Y, Liu L, Huang E, Deng C, Luo C, Han M, Chen P, et al. IL-17 drives salivary gland dysfunction via inhibiting TRPC1-mediated calcium movement in Sjögren's syndrome. Clin Transl Immunol. 2021;10: e1277.
78. Verstappen GM, Kroese FGM, Bootsma H. T cells in primary Sjögren's syndrome: targets for early intervention. Rheumatology. 2021;60:3088–98.
79. Harbour SN, DiToro DF, Witte SJ, Zindl CL, Gao M, Schoeb TR, Jones GW, Jones SA, Hatton RD, Weaver CT. T(H)17 cells require ongoing classic IL-6 receptor signaling to retain transcriptional and functional identity. Sci Immunol. 2020;5:eaaw2262.
80. Xu L, Kitani A, Strober W. Molecular mechanisms regulating TGF-beta-induced Foxp3 expression. Mucosal Immunol. 2010;3:230–8.

81. Lin X, Wang X, Xiao F, Ma K, Liu L, Wang X, Xu D, Wang F, Shi X, Liu D, et al. IL-10-producing regulatory B cells restrain the T follicular helper cell response in primary Sjögren's syndrome. Cell Mol Immunol. 2019;16:921–31.
82. Warren RB, Blauvelt A, Bagel J, Papp KA, Yamauchi P, Armstrong A, Langley RG, Vanvoorden V, De Cuyper D, Cioffi C, et al. Bimekizumab versus adalimumab in plaque psoriasis. N Engl J Med. 2021;385:130–41.
83. Oliver R, Krueger JG, Glatt S, Vajjah P, Mistry C, Page M, Edwards H, Garcet S, Li X, Dizier B, et al. Bimekizumab for the treatment of moderate-to-severe plaque psoriasis: efficacy, safety, pharmacokinetics, pharmacodynamics and transcriptomics from a phase IIa, randomized, double-blind multicentre study. Br J Dermatol. 2022;186:652–63.
84. Glatt S, Taylor PC, McInnes IB, Schett G, Landewé R, Baeten D, Ionescu L, Strimenopoulou F, Watling MIL, Shaw S. Efficacy and safety of bimekizumab as add-on therapy for rheumatoid arthritis in patients with inadequate response to certolizumab pegol: a proof-of-concept study. Ann Rheum Dis. 2019;78:1033–40.
85. van der Heijde D, Gensler LS, Deodhar A, Baraliakos X, Poddubnyy D, Kivitz A, Farmer MK, Baeten D, Goldammer N, Coarse J, et al. Dual neutralisation of interleukin-17A and interleukin-17F with bimekizumab in patients with active ankylosing spondylitis: results from a 48-week phase IIb, randomised, double-blind, placebo-controlled, dose-ranging study. Ann Rheum Dis. 2020;79:595–604.

Publisher's Note